# The Effective Impedance of a Finite-Thickness Viscothermal Boundary Layer Over an Acoustic Lining

Doran Khamis* and Edward J. Brambley†

*University of Cambridge, UK*

**This paper assesses the importance of viscothermal effects for acoustics calculations in lined ducts, both inside and outside of a finite-thickness compressible boundary layer using a combination of asymptotics and numerics.**

**Viscosity is always present, even at the high Reynolds numbers associated with aeroacoustics. The large majority of aeroacoustic calculations are performed inviscidly, however. Existing inviscid impedance boundary conditions (e.g. Myers) have failed in predicting experimental results, and it is suggested that viscosity is the key to accurate computations. Here, numerical solutions of the Linearized Navier–Stokes equations are compared to inviscid numerics inside a sheared boundary layer to quantify the errors associated with neglecting viscosity. It is found that invisicd errors are strongly dependent on frequency, with normalised errors of over 10% common at low frequencies. It is suggested that errors increase with Mach number, though the dependence is weaker than that of frequency. Viscothermal effects are also shown to be as important as shear.**

**Existing impedance boundary conditions rely on the assumption that the acoustics outside the boundary layer are the same as they would be in a completely uniform inviscid flow. This assumption, that the near-wall effects of shear and viscous dissipation do not penetrate far into the duct, is tested here by comparing analytic expressions for the uniform acoustics with viscous numerics. It is found that errors outside a 99% boundary layer are on average 0.006% for the pressure and 0.1% for the radial velocity, validating this assumption**

**Three existing impedance boundary conditions are tested against full viscous numerics and are found to be inadequate for modelling the possibly unstable surface modes. A new asymptotic boundary condition is derived that combines the regularising effect of a finite-thickness shear layer with viscosity and thermal conduction to accurately capture the physics of a boundary layer over an acoutic lining. Comparisons of the new boundary condition with viscous numerics are extremely positive, and due to the decoupling of the Reynolds number and boundary layer thickness in the derivation the condition may be used for any flow. The new condition correctly predicts the stability of modes as parameters vary. Though an analytic form of the new condition is not found, it is suggested that it could be incorporated into a boundary solver at minor computational cost.**

## Nomenclature

| | | | |
|---|---|---|---|
| $\rho$ | Density | $r$ | Radial coordinate |
| $T$ | Temperature | $x$ | Axial coordinate |
| $p$ | Pressure | $\theta$ | Azimuthal coordinate |
| $\mathbf{u}$ | Velocity vector | $\mathbf{e_x}$ | Axial unit vector |
| $u$ | Radial velocity | $\mathbf{e_r}$ | Radial unit vector |
| $v$ | Axial velocity | $\omega$ | Angular frequency |
| $w$ | Azimuthal velocity | $k$ | Axial wavenumber |
| $\mathbf{r}$ | Position vector | $m$ | Azimuthal wavenumber |

*PhD Student, Department of Applied Mathematics and Theoretical Physics, University of Cambridge, Centre for Mathematical Sciences, Wilberforce Road, Cambridge CB3 0WA, United Kingdom. AIAA member.

†Research Fellow, Department of Applied Mathematics and Theoretical Physics, University of Cambridge, Centre for Mathematical Sciences, Wilberforce Road, Cambridge CB3 0WA, United Kingdom. AIAA member.

| | |
|---|---|
| $\mu$ | Shear viscosity |
| $\mu^B$ | Bulk viscosity |
| $\kappa$ | Thermal conductivity |
| $c_0$ | Centreline sound speed |
| $l$ | Characteristic duct dimension |
| $c_p$ | Specific heat at constant pressure |
| $\gamma$ | Ratio of specific heats |
| $M$ | Mach number |
| $\delta$ | Boundary layer thickness |
| Re | Reynolds number |
| Pr | Prandtl number |
| $\sigma$ | Viscous stress tensor |
| $D$ | Eulerian rate of strain tensor |
| $\beta$ | Second coefficient of viscosity |
| $Z$ | Reduced impedance |
| $Z_{\text{eff}}$ | Effective reduced impedance |
| $A$ | Variable matrix |
| $\mathbf{x}$ | Solution vector |
| $\mathbf{b}$ | Variable vector |
| $y$ | Boundary layer coordinate |
| $Y$ | Finite truncation of boundary layer |
| $y_B$ | Point where Blasius velocity reaches $0.76M$ |
| $N$ | Number of finite difference grid points |
| $C_N$ | Number of grid points outside boundary layer |
| $r_m$ | Set of radial coordinates outside boundary layer |
| $r_j$ | $j$th radial grid point |
| $\chi$ | Normalised Root Mean Square Error |
| $J_m$ | Cylindrical Bessel function of the first kind, of order $m$ |
| $h$ | Square root of Prandtl number |
| $\eta$ | Branch of $\sqrt{i(\omega - Mk)}$ |
| $\xi$ | Viscothermal parameter linking Re and $\delta$ |
| $\text{Re}(q)$ | Real part of quantity |
| $\text{Im}(q)$ | Imaginary part of quantity |
| $q^*$ | Dimensional quantity |
| $q_0$ | Centreline base quantity |
| $\tilde{q}$ | Acoustic quantity |
| $q_{\text{u}}$ | Uniform flow acoustic quantity |
| $\hat{q}$ | Rescaled acoustic quantity |
| $q_\infty$ | Uniform flow acoustic quantity evaluated at lined wall |
| $q^{(j)}$ | $j$th term in asymptotic expansion of quantity |
| $q^j$ | $q(r_j)$, quantity evaluated at $j$th grid point |

## 1. Introduction

The majority of studies in the literature concerning sound propagation in a duct assume the carrier fluid to be inviscid. This allows the acoustic pressure field to be simply expressed in uniform flow [1], and analytic approximations of this field to be extended into regions of shear (i.e. boundary layers) [2–8]. This paper aims to assess the importance of viscosity with regards to the use of effective impedance boundary conditions (combining the impedances of the lining and the boundary layer), which approximate the behaviour of the acoustics in a sheared boundary layer over an acoustic lining. It is already known that the inclusion of viscosity in computations leads to better agreement with experiment in some circumstances [9–11], and it has been shown in previous expeimental studies that the classical inviscid Myers condition is fallible [12–14]. Here, the idea that inviscid equations can really model the physics of a strongly sheared boundary layer over an acoustic lining is questioned by comparing Linearized Navier–Stokes (LNS) with inviscid computations inside the base flow shear layer.

Previous studies which have included viscous effects in an effective impedance boundary condition [15–17] have various shortcomings, as will be discussed – in particular, the leading order viscous corrections to the Myers condition [17] do not regularise its ill-posedness. In these studies the effects of viscosity are assumed to be localised to the boundary layer. This assumption will be tested by comparing numerical solutions of the LNS in the core of a duct (i.e. outside the boundary layer) with analytic expressions for the acoustics in a uniform, slipping flow.

Existing effective impedance boundary conditions will be compared with LNS numerics. The illposed [18] yet widely used Myers condition [19,20], and the regularisation of this condition [6,7] (here called the Modified Myers condition), as well as the viscous condition of Brambley [17], will be tested. In particular, how these boundary conditions describe the behaviour of the possible instability modes, inherent in the use of acoustically soft walls, will be investigated. It has been shown that for an inviscid shear layer over an acoustic lining there exists surface modes (oscillations at or near the boundary) that can become unstable. When excited, an unstable surface mode has been shown to be convectively unstable (growing in space), or, under certain circumstances, absolutely unstable (growing in both time and space) [21–25]. (These surface mode instabilities are different from the vortex sheet instability of the Myers condition, which is regularised by considering a finite shear layer.) Inviscid computations concerning the proposed hydrodynamic instability mode [21] were compared well in Ref. 26 to the experimental data of Ref. 13, though the growth rate of the theoretical instability was appreciably higher than the experimentally observed instability, suggesting viscous damping plays a role.

Having ascertained the importance of viscosity for predictions of sound fields and stability analyses, the

LNS are analysed asymptotically by expanding in a finite boundary layer thickness $\delta$. A reduced system of equations is derived which describes the acoustic field inside the sheared boundary layer over an acoustic lining. By solving this system numerically it is shown that it is possible to improve upon the predictions of the effective impedances made by the existing models (both inviscid and viscous). An explicit boundary condition is not found, but it is suggested that the reduced system could be incorporated into a boundary solver.

## 2. Governing equations

### A. Nondimensionalisation

We imagine a duct with an inviscid, uniform base flow at its centreline. Then, where a star denotes a dimensional variable, we nondimensionalise densities by the base centreline value, $\rho^* = \rho_0^* \rho$; velocities by the centreline sound speed, $\mathbf{u}^* = c_0^* \mathbf{u}$; lengths by the characteristic duct dimension (i.e. its radius), $\mathbf{r}^* = l^* \mathbf{r}$; and temperatures by $T^* = c_0^{*2}/c_p^* T$, where $c_p^*$ is the specific heat at constant pressure. Continuing, we scale pressure and viscous stress by $c_0^{*2}\rho_0^*$; coefficients of viscosity by $c_0^* l^* \rho_0^*$; thermal conductivity by $c_0^* l^* \rho_0^* c_p^*$; and time by $l^*/c_0^*$. In such a scheme, the centreline base flow density, temperature and pressure take the respective values $\rho_0 = 1$, $T_0 = 1/(\gamma - 1)$ and $p_0 = 1/\gamma$, where $\gamma$ is the ratio of specific heats. The dimensionless core velocity is $U_0 = M$, the centreline Mach number of the flow. The viscosities and thermal conductivity are taken to depend linearly on temperature over the relevant temperature range, meaning their small variations introduce perturbations comparable to the acoustic temperature field.

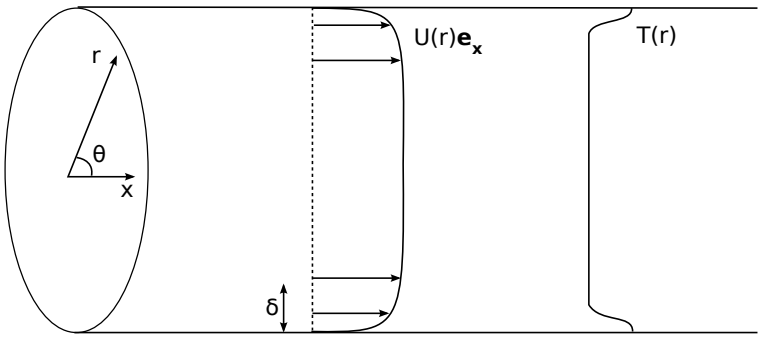


Figure 1. Schematic of lined cyclindrical duct with radially varying temperature and parallel flow

To gear our analysis to applications inside aeroengines we work in cylindrical coordinates $(r, \theta, x)$. The domain is then a cylindrical shell of infinite axial extent (no leading- or trailing-edge effects) with dimensionless radius $r = 1$ (see Figure 1). This is divided into two regions: (i) the core of the flow, occupying $0 \leq r \leq 1-\delta$, in which the flow is moving with a uniform (or close to uniform) velocity; and (ii) the boundary layer, occupying $1-\delta < r < 1$, where the effects of viscosity and thermal conduction cause strong shear and temperature/density gradients. Here, $\delta$ is the dimensionless boundary layer thickness, ranging in our computations from $10^{-4}$ to $10^{-1}$. It is assumed that we are studying a steady-state laminar boundary layer far downstream from leading edges, and that the base flow is at all points parallel with the duct wall. In the core of the flow, the base flow dynamical variables take the constant zero-subscripted values stated above. In the boundary layer, the base flow variables follow some $r$-dependent profile such that no-slip and isothermal boundary conditions are satisfied at the lining.

The Reynolds number Re, often scaled out of the equations through a relationship with the boundary layer thickness, is kept in the system here as a separate parameter. This allows the acoustics to be investigated over a large range of Re–$\delta$ parameter space, and for the effect of each parameter to be tested separately. We define the Reynolds number with respect to the centreline sound speed, $\mathrm{Re} = c_0^* l^* \rho_0^*/\mu_0^*$. The Prandtl number is similarly defined by centreline variables, $\mathrm{Pr} = \mu_0^* c_p^*/\kappa_0$. These definitions allow the viscosity and thermal conductivity to be expressed in terms of Pr and Re as

$$\mu = \frac{T}{T_0 \mathrm{Re}}, \qquad \mu_B = \frac{T}{T_0 \mathrm{Re}} \frac{\mu_0^{B*}}{\mu_0^*}, \qquad \kappa = \frac{T}{T_0 \mathrm{RePr}}, \tag{2.1}$$

where $\mu^B$ is the bulk viscosity.

### B. Viscous compressible fluid equations

We are concerned with the dynamics of a viscous compressible gas, for which the stress tensor takes the form

$$\sigma_{ij} = 2\mu D_{ij} + \beta \nabla \cdot \mathbf{u} \delta_{ij}. \tag{2.2}$$

Here, $D$ is the Eulerian rate of strain tensor $2D_{ij} = (\partial u_i/\partial x_j + \partial u_j/\partial x_i)$; $\mu$ and $\beta$ are the dynamic and *second*[27] viscosity respectively, where $\beta$ is related to the bulk viscosity $\mu^B$ by $\beta + 2\mu/3 = \mu^B$. It is posited that the energy dissipation due to the viscous stresses and thermal conduction occurs only (or rather, mainly) inside the thin boundary layer near a surface (this will be tested later). The full nondimensional governing equations are[28,29]

$$\frac{\partial \rho}{\partial t} + \nabla \cdot (\rho \mathbf{u}) = 0, \tag{2.3a}$$

$$\rho \frac{D\mathbf{u}}{Dt} = -\nabla p + \nabla \cdot \sigma, \tag{2.3b}$$

$$\rho \frac{DT}{Dt} = \frac{Dp}{Dt} + \nabla \cdot (\kappa \nabla T) + \sigma_{ij} \frac{\partial u_i}{\partial x_j}, \tag{2.3c}$$

$$T = \frac{\gamma}{\gamma - 1} \frac{p}{\rho}, \tag{2.3d}$$

in which the material derivative is $D/Dt = \partial/\partial t + \mathbf{u} \cdot \nabla$.

We linearise equations (2.3) about the base flow to arrive at the LNS, with acoustic quantities having the harmonic dependence $\exp\{i\omega t - ikx - im\theta\}$. The LNS are solved in the domain $r \in [0, 1]$, with regularity conditions applied to the acoustics at the duct centreline $r = 0$. At the lined wall $r = 1$, the axial base flow $U$ satisfies no-slip, as do the axial and azimuthal acoustic velocities $\tilde{u}$ and $\tilde{w}$. Isothermal boundary conditions are also applied, such that the base temperature, $T$, has zero gradient at the wall, and the temperature perturbation, $\tilde{T}$, is zero at the wall. At the lining, the acoustic pressure $\tilde{p}$ drives a radial velocity $\tilde{v}$ via an impedance $Z$: $\tilde{p}(1) = Z\tilde{v}(1)$ (equivalent to the Myers boundary condition due to the no slip at the wall).

## 3. Numerical method

The LNS as derived forms a system of five equations for five unknowns, $(\tilde{p}, \tilde{u}, \tilde{v}, \tilde{w}, \tilde{T})$, once the density has been eliminated using the constitutive law (2.3d). We discretise the domain such that the physical $r$ space has $N$ unevenly spaced points, with more points clustered in the boundary layer to fully resolve the behaviour there. The physical space is then mapped onto an evenly spaced computational grid, $\xi$, allowing the numerical derivatives to be performed more stably. The relationship

$$\frac{\mathrm{d}}{\mathrm{d}r} = \frac{\partial \xi}{\partial r} \frac{\mathrm{d}}{\mathrm{d}\xi} \tag{3.1}$$

is used to map the $r$ derivatives to the computational domain, where $\xi$ and $r$ are related by

$$r = \frac{\tanh S\xi}{\tanh S}. \tag{3.2}$$

Here, $S$ is a stretching parameter. Higher values of $S$ allow more points to be clustered near $r = 1$, and $S$ was chosen to give at least 400 points in the boundary layer for any $\delta$.

The resulting linear system is of the form $A\mathbf{x} = \mathbf{b}$, where $A$ is a $5N \times 5N$ sparse matrix and $b$ is a vector of zeros bar one entry in which we set the boundary condition $\tilde{p}(1) = 1$ to force a non-zero solution. We use a 6th order, unoptimised[30], central finite difference discretisation on the uniform computational grid to approximate the derivatives in $A$. The system is first order in $\tilde{p}$ and second order in $\tilde{u}$, $\tilde{v}$, $\tilde{w}$ and $\tilde{T}$ so we may apply nine boundary conditions: we choose to apply a regularity condition on all five variables at $r = 0$, and leave $\tilde{v}$ unconstrained at the lining $r = 1$. This leaves the dispersion relation still to be satisfied, as described below. The system is solved with a sparse matrix solver for the solution vector $\mathbf{x}$.

### A. Mode finding and the effective impedance

Since $\tilde{v}$ is left unconstrained at the boundary, we must use Newton-Raphson iteration to apply the desired impedance boundary condition at $r = 1$. In this way, $(k, \omega)$ modes are found for a given azimuthal wavenumber $m$ by iterating to solve the dispersion relation

$$\frac{\tilde{p}(1)}{\tilde{v}(1)} = Z, \tag{3.3}$$

where $Z$ may either take a specified value, or depend on $\omega$ or $k$ through some liner model (such as a mass-spring-damper or Helmholtz resonator model).

Our definition of effective impedance is that impedance $Z_{\text{eff}}$ which, applied as an acoustic boundary condition for a uniform, inviscid slipping duct flow, produces the uniform acoustic fields $\tilde{q}_{\text{u}}$ that match the viscous, sheared acoustics outside the boundary layer. That is, applying the condition

$$\frac{\tilde{p}_{\text{u}}(1)}{\tilde{v}_{\text{u}}(1)} = Z_{\text{eff}}, \tag{3.4}$$

should allow $\tilde{p}_{\text{u}} \approx \tilde{p}$ for $0 < r < 1 - \delta$. The assumption made during previous attempts at finding such an effective impedance[7,8,20] is that this is possible. This will be tested in the next section. For an inviscid flow and a vortex sheet-boundary layer, the Myers $Z_{\text{eff}}$ may be derived:

$$Z_{\text{myers}} = \frac{\omega}{\omega - Mk} Z. \tag{3.5}$$

The Modified Myers condition adds $\mathcal{O}(\delta)$ terms to (3.5) to account for a finite-thickness boundary layer, while the leading order viscous condition of Ref. 17 reduces to (3.5) (numerically) if the viscosity and thermal conduction are set to zero.

The acoustic pressure in a uniform slipping flow satisfies a form of Bessel's equation,

$$\frac{\mathrm{d}^2\tilde{p}_{\text{u}}}{\mathrm{d}r^2} + \frac{1}{r}\frac{\mathrm{d}\tilde{p}_{\text{u}}}{\mathrm{d}r} + \left((\omega - Mk)^2 - k^2 - \frac{m^2}{r^2}\right)\tilde{p}_{\text{u}} = 0, \tag{3.6}$$

where we have taken $\rho(r) \equiv 1$ and $U(r) \equiv M$. Equation (3.6) may be solved in terms of Bessel functions,

$$\tilde{p}_{\text{u}}(r) = E J_m(\alpha r), \qquad \alpha^2 = (\omega - Mk)^2 - k^2, \tag{3.7}$$

and the inviscid Euler equations may be used to find the related acoustic radial velocity,

$$\tilde{v}_{\text{u}}(r) = \frac{iE\alpha J_m'(\alpha r)}{\omega - Mk}, \tag{3.8}$$

where a prime denotes a derivative with respect to the argument. Using (3.7) and (3.8), then, it is possible to form explicitly the effective impedance from (3.4):

$$Z_{\text{eff}} = (\omega - Mk)\frac{J_m(\alpha)}{i\alpha J_m'(\alpha)}. \tag{3.9}$$

Importantly, the normalisation constant $E$ drops out when the ratio of $\tilde{p}_{\text{u}}$ and $\tilde{v}_{\text{u}}$ is taken. This means that the value of $Z_{\text{eff}}$ for a given Mach number $M$ is only dependent on the triplet $(k, \omega, m)$, and not on the amplitude of the acoustics.

### B. Base flow

Up to this point we have made no assumptions about the boundary layer profile of the base flow, other than that it must depend only on $r$. It is unclear as to what the character of the boundary layer inside a real aircraft engine intake is. Common velocity profiles used in the literature include power law, sinusoidal, logarithmic, and linear. It has been shown that the actual profile of the base flow is not as important to sound attenuation calculations as parameters such as the displacement or momentum thickness[31,32], so results found using a single base profile can be considered, in part, to be universal. However, it has been

shown that the profile can affect the number of surface modes predicted by a model[25], so the profile chosen may have important ramifications for the stability of the boundary layer. Care must be taken also to ensure that the chosen base profile satisfies the desired physics: here, we assume the wall and fluid are in thermal equilibrium, so $T_r(1) = 0$ must hold for any base profile.

A compressible Blasius flat-plate boundary layer[33] of thickness $\delta$ ($10^{-4}$–$10^{-1}$) is used for most of the subsequent computations (see Ref. 34 for details). This is to ensure that a 'realistic' interplay between temperature and velocity is captured in the boundary layer (the focus, afterall, being on viscothermal effects). Hence, an $r$-dependent temperature profile is required, as well as a velocity profile.

The Blasius equations were solved on the end section of the stretched physical domain $r \in [1 - \delta Y/y_B, 1]$, mapped to the boundary layer variable $y \in [0, Y]$. The value of $y_B$ is the point in the $y$ domain where the Blasius velocity reaches $0.76M$, and is dependent on the Mach number. The $0.76M$ value is taken from the common tanh velocity profile used in Refs. 25,26,35, which is defined below in (5.1). The value $Y$ was chosen such that the conditions at infinity were suitably satisfied, and such that the matching to the uniform flow in the core of the duct was sufficiently smooth. Most computations herein use the value $Y = 23$ which produces a boundary condition error of $10^{-10}$. By scaling the boundary layer by $Y/y_B$, we provide enough 'room' in our duct domain for the Blasius profile solver such that the desired boundary layer thickness convention is adhered to. We calculate the base flow at leading order only, as the corrections at $\mathcal{O}(\delta)$ from the cylindrical geometry and boundary layer scaling are considered sub-dominant. We note that if they were included in the analysis, the cross-flow $V$ term, appearing at the same order, must also be included, as must the slow variation of $\delta$ with axial distance $x$. The Blasius boundary layer is a function of $y/\sqrt{x}$; we use the argument made in Ref. 34 that solutions for a fixed axial coordinate (we choose here $x = 1$) are universal.

## 4. Numerical comparisons: viscous vs. inviscid

The reporting of take-off and flight conditions at the inlet of an aeroengine varies greatly. The Reynolds number lies in the range $10^5$-$10^7$, and the Mach number is between 0.3 and 0.7, depending on the study. We will try here to aim for mild generality, and investigate the effects of all (most) parameters on the acoustics in a lined duct.

To do this, we begin by comparing LNS computations with those from the same solver but with viscosity set to zero (i.e. the inviscid Euler equations, which reduce to the Pridmore-Brown equation[36], henceforth PB). This will help elucidate whether (i) viscosity is important in calculating the effect of a 'soft' lining on the acoustics in a boundary layer; and (ii) whether its effects are localised near the boundary, and hence whether the hypothesis of applying a viscous boundary condition to a inviscid flow has merit.

### A. Inside the boundary layer

Although the pressure field is usually what people are interested in when discussing acoustics, we also consider here the acoustic radial velocity. This is because both the viscous and inviscid numerics adhere to the boundary condition $\tilde{p}(1) = 1$, hence any variation of pressure inside the boundary layer is muted by the boundary forcing.

Figure 2 shows the real and imaginary parts of the acoustic radial velocity inside the boundary layer as frequency is reduced (left to right) for fixed $k$, $\delta$, $M$, $m$ and Re. Plotted are the full, sheared LNS results, sheared PB results, and, for comparison, uniform slipping PB results. The higher-frequency results ($\omega = 31$ and $\omega = 15$) in Figures 2a and 2b show that the viscothermal acoustics (solid) deviate from the inviscid acoustics (dashed) only slightly through the boundary layer, with the largest deviation tending to be very close to the wall (the acoustic boundary layer). This is in stark contrast to the lower-frequency results ($\omega = 5$) in Figure 2c, where viscosity is having a large effect on the acoustics throughout the base flow boundary layer, and the behaviour is qualitatively different, in line with predictions in Refs. 16,17. Comparing the values at the wall ($r = 1$) of the three solutions (viscous, inviscid, and uniform inviscid) in Figs. 2a and 2c, we see that the magnitude of the viscous effect is of the same order as that of the shear. Figure 3 shows similar results for a variety of parameters, displaying just the sheared results. Importantly, Fig 3b shows a situation where viscothermal effects force of a non-zero real part of the radial velocity where the inviscid counterpart is purely imaginary. (This of course depends upon the normalisation chosen, and can occur when both the frequency and axial wavenumber are real.)

To quantify the errors of the the inviscid acoustics, we must use an applicable definition of normalised

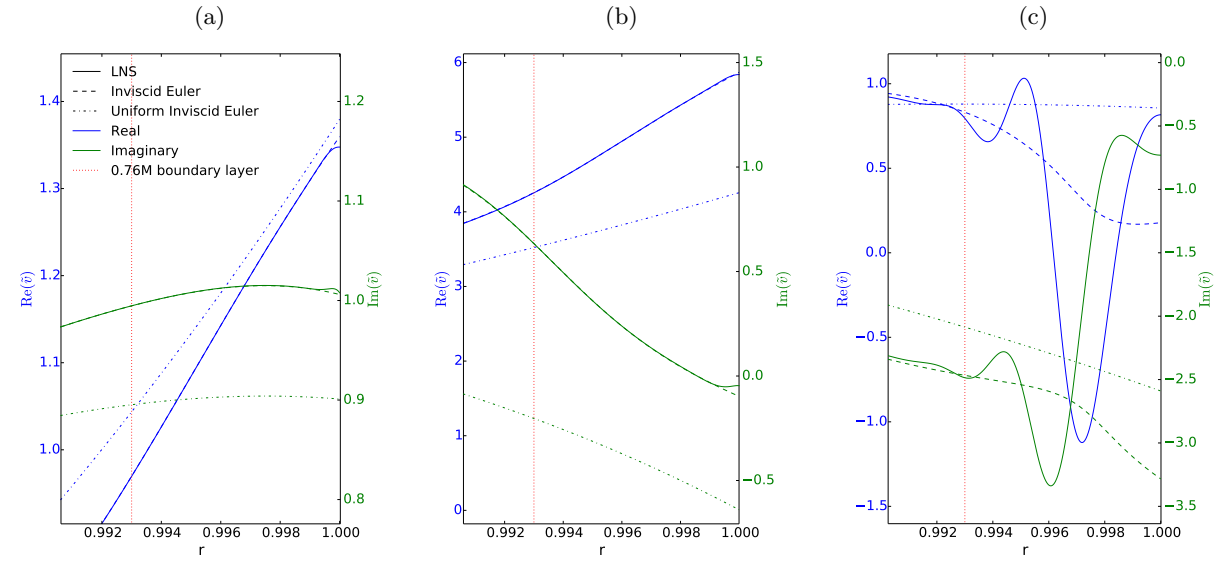


Figure 2. Close-ups for the boundary layer showing the real and imaginary part of the acoustic radial velocity for the LNS (solid), PB (dashed) and uniform PB (dash-dot). In (a) $\omega = 31$, (b) $\omega = 15$, (c) $\omega = 5$. $k = 26 - 14i$, $m = 12$, $M = 0.5$, $\delta = 7 \times 10^{-3}$, $\mathrm{Re} = 1 \times 10^{6}$.

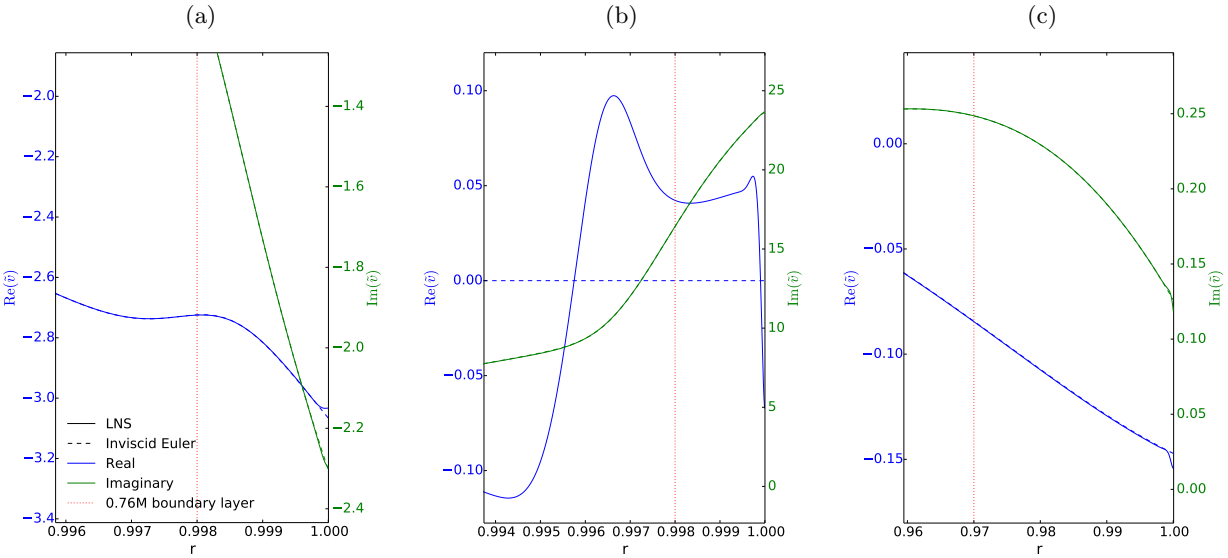


Figure 3. Close-ups for the boundary layer showing the real and imaginary part of the acoustic radial velocity for the LNS (solid) and PB (dashed). (a) $\omega = 31$, $k = 41 + 25i$, $m = 0$, $M = 0.7$, $\delta = 2 \times 10^{-3}$, $\mathrm{Re} = 1 \times 10^{7}$; (b) $\omega = 31$, $k = 60$, $m = 24$, $M = 0.5$, $\delta = 2 \times 10^{-3}$, $\mathrm{Re} = 1 \times 10^{7}$; (c) $\omega = 31$, $k = 12 + 2i$, $m = 24$, $M = 0.3$, $\delta = 3 \times 10^{-2}$, $\mathrm{Re} = 5 \times 10^{5}$

error. Since the real and imaginary parts of $\tilde{p}$ and $\tilde{v}$ often pass through zero, the relative error throws anomalous results. We cannot simply consider the relative error of the absolute values as the inviscid and viscous solutions sometimes have different signs – taking the absolute value would disregard the sign change and hence the error would be underestimated. We must forgo relative error altogether and consider absolute error, which we make 'relative', in a broad sense, by normalising with respect to the mean value of the viscous solution throughout the boundary layer. This error definition has difficulties if the mean value throughout the boundary layer is close to zero, as this can cause the error to be exagerated. Examples of this normalised error are shown in Figures 4, 5 and 6. Figure 4 shows that substantial errors are common for low and moderate frequencies ($\omega = 5, 15$ are the top two rows). Merely increasing the azimuthal wavenumber and

thickening the boundary layer suppresses most of the large errors at the moderate frequency ($\omega = 15$), as can be seen in Fig. 5. Both Figure 4 and 5 suggest that an increase in Mach number (left to right) leads to an increase in error in the inviscid approximation, as found in the experiments of Ref. 39. Figure 6 shows the fragility of the inviscid approximation: changing the wavenumber from $k = 41 + 25i$ to $k = 26 - 14i$, with all else held constant, introduces massive errors when oscillatory viscous modes are excited in the boundary layer. The exact size of the large errors visible in Fig. 6 should not be taken as writ due to the noted problems with the normalisation, but the general trend is important. The conclusion to draw from these three collections of plots is that for very realisable parameter sets, it is often the case that inviscid acoustics in a sheared boundary layer at a lining are appreciably wrong when compared with the viscous acoustics. There are exceptions to this, in which certain parameter sets have small errors close to 1%, or in which massive errors of over 100% occur, but it is difficult to discern trends that help to predict when these exceptions will happen. Viscosity, then, is important for the accurate prediction of acoustic modeshapes inside the mean flow boundary layer at a lined wall.

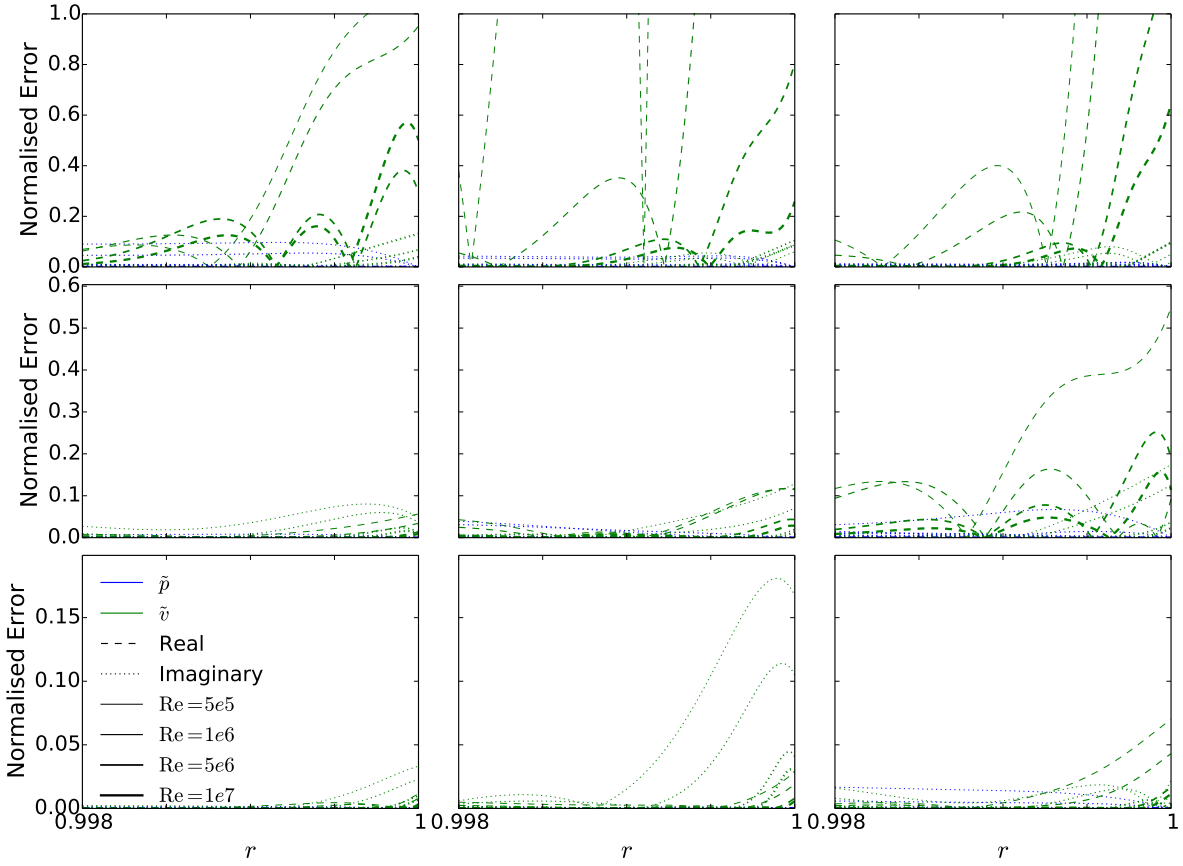


Figure 4. The normalised error of the inviscid acoustics with respect to the viscous acoustics. The rows have frequencies $\omega = 5$, 15 and 31 respectively; the columns have Mach numbers $M = 0.3$, 0.5, 0.7 respectively. Reynolds number increases with line thickness in Re $\in [5e5, 1e6, 5e6, 1e7]$. Green lines are for $\tilde{p}$, blue lines are for $\tilde{v}$; dashed shows real parts, dotted shows imaginary parts. Fixed paramters are $k = 41 + 25i$, $m = 0$ and $\delta = 2e$-3.

As an easily comparable measure of accuracy, the boundary layer mode shapes are used to calculate the Normalised Root Mean Square Error (NRMSE, $\chi$, defined in (4.1) below) of the inviscid solution compared to the LNS. Then, 972 parameter sets (detailed in Table 1) are tested. By calculating bulk values of the mean, maximum and minimum error, a more general view is attained of the error associated with the inviscid approximation. Table 1 shows the expected trend that higher Reynolds numbers make for a 'more inviscid' flow. The mean error through the boundary layer for the acoustic pressure is 2.5% for the moderate Reynolds number of $5 \times 10^5$, while for the high Reynolds number of $1 \times 10^7$ the mean error reduces to 1.1%. The radial velocity sees a larger reduction, from 11% to 3.2%. The results for different Mach numbers are shown in Table 2, in which the $\tilde{v}$ results lend weight to the hypothesis that errors increase with Mach number. This

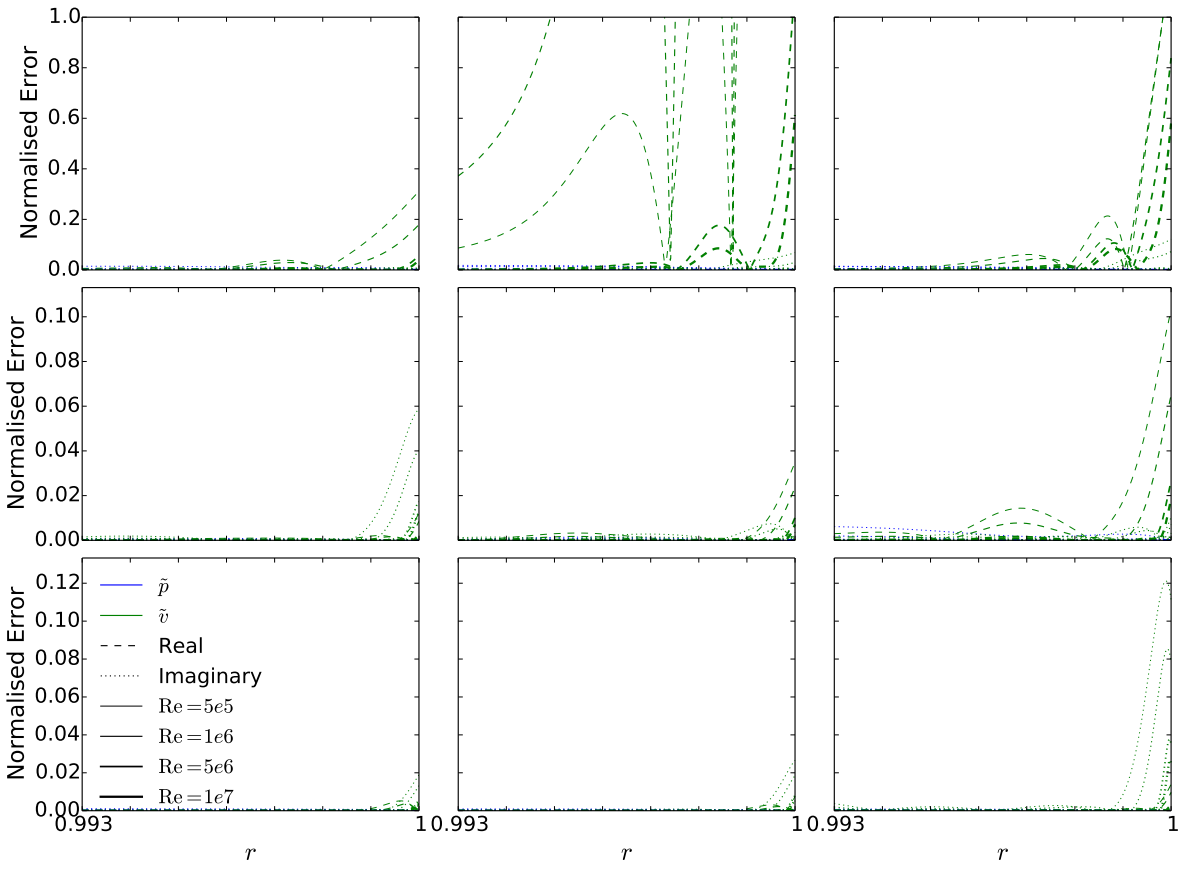


Figure 5. As Figure 4 but with $m = 12$ and $\delta = 7e\text{-}3$.

| | $\chi(\tilde{p})$ | | | $\chi(\tilde{v})$ | | |
|---|---|---|---|---|---|---|
| Re | Mean | Max | Min | Mean | Max | Min |
| 5e5 | 0.025 | 0.51 | 9.3e-6 | 0.11 | 0.84 | 0.0013 |
| 1e6 | 0.018 | 0.37 | 5.0e-6 | 0.083 | 0.73 | 8.4e-4 |
| 5e6 | 0.012 | 0.38 | 1.1e-6 | 0.043 | 0.59 | 2.9e-4 |
| 1e7 | 0.011 | 0.41 | 5.5e-7 | 0.032 | 0.53 | 1.8e-4 |

Table 1. Bulk analysis of 972 parameter sets for which the Normalized Root Mean Square Error (NRMSE) was calculated for both $\tilde{p}$ and $\tilde{v}$ over the boundary layer. The mean, maximum and minimum of the NRMSE are shown here for various values of the Reynolds number. All permutations of the following parameters were used: $\omega \in [5, 15, 31]$, $k \in [12 + 2i, 41 + 25i, 26 - 14i]$, $m \in [0, 12, 24]$, $M \in [0.3, 0.5, 0.7]$, $\delta \in [2e\text{-}3, 7e\text{-}3, 3e\text{-}2]$ and $\mathrm{Re} \in [5e5, 1e6, 5e6, 1e7]$.

bulk treatment also allows a clearer picture to be painted of the dependency upon frequency of the inviscid error: the mean $\tilde{v}$ errors are 16%, 3.2% and 1.2% for $\omega = 5$, 15 and 31 respectively. To conclude, it is difficult to predict for what values of $k$, $m$, and $\delta$ viscosity will play a substantial role – it is clear, however, that it very often does, and that the inviscid errors are strongly dependent on frequency and weakly dependent on Mach number.

## B. Outside the boundary layer

The hope of those working with boundary conditions for lined ducts is that near-wall effects (viscosity, thermal conduction, strong shear) do not penetrate far into the duct core. Then, it is reasoned, the physics of these effects may be collapsed into a single boundary condition. This condition would be applicable, at a lined wall, to a flow that suffers from none of said near-wall effects (for instance, an inviscid uniform slipping

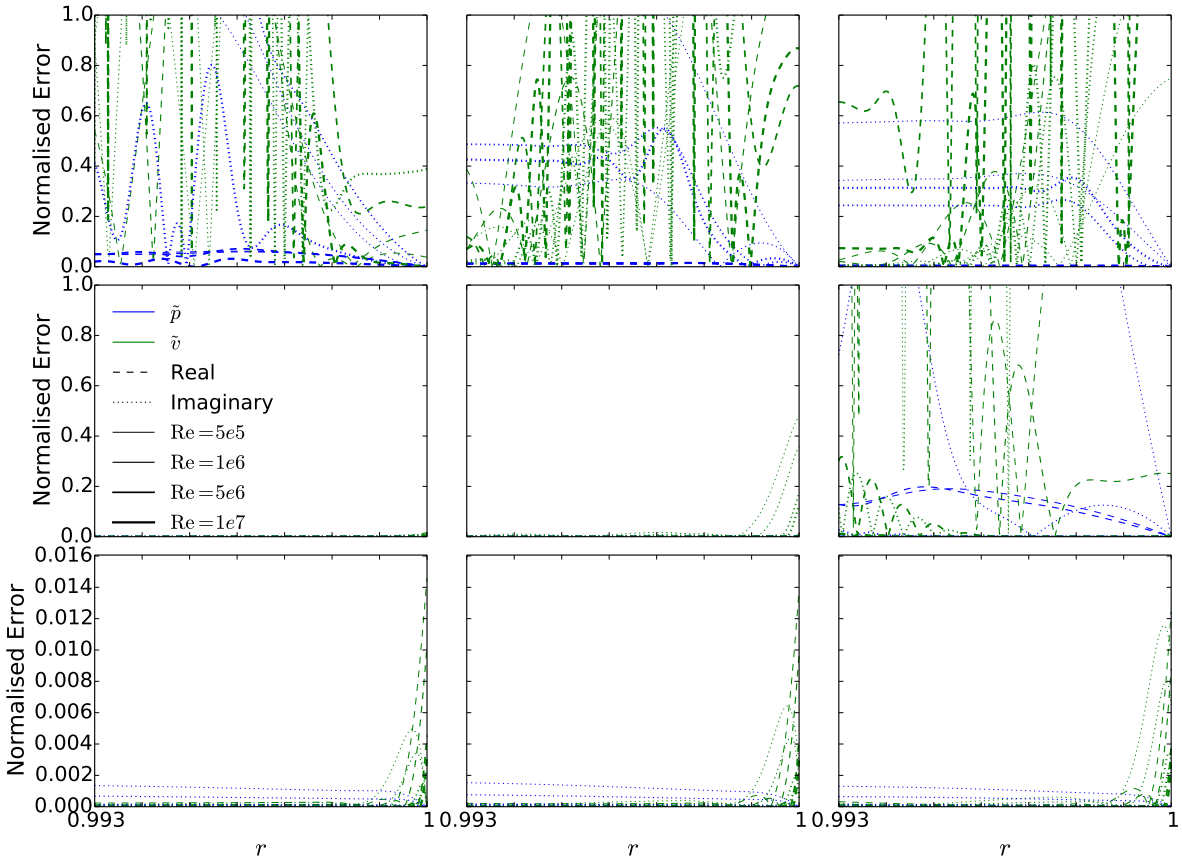


Figure 6. As Figure 5 but with $k = 26 - 14i$.

| | $\chi(\tilde{p})$ | | | $\chi(\tilde{v})$ | | |
|---|---|---|---|---|---|---|
| $M$ | Mean | Max | Min | Mean | Max | Min |
| 0.3 | 0.012 | 0.30 | 5.5e-7 | 0.053 | 0.82 | 1.8e-4 |
| 0.5 | 0.010 | 0.22 | 1.3e-6 | 0.067 | 0.84 | 2.0e-4 |
| 0.7 | 0.027 | 0.51 | 1.3e-6 | 0.084 | 0.79 | 2.3e-4 |

Table 2. As in Table 1, but showing the mean, maximum and minimum NRMSE for various Mach numbers.

flow). Here we assess this hope. To do this, the uniform pressure solution, $\tilde{p}_\mathrm{u}$, from equation (3.7) is matched to the full LNS solution for a given parameter set, and the error *outside* the boundary layer calculated. The matching is performed numerically at a set of radial positions $r_m$ by iterating the normalisation constant $E$, in (3.7), to minimise the expression $1-\tilde{p}_\mathrm{u}(r_j)/\tilde{p}(r_j)$, where $r_j \in r_m$. Then, $\chi(\tilde{p}_\mathrm{u})$ over the core of the duct is calculated for each matching point in $r_m$. The minimum of these errors then gives an approximation of how well the LNS acoustics are approximated by the invisicd, uniform flow acoustics outside the boundary layer. We define *outside* the boundary layer here as where there is almost no shear. We adopt the 99% boundary layer convention for this purpose – that is, the base flow velocity for all $r_j \in r_m$ satisfies $U(r_j) \geq 0.99M$, for the core Mach number $M$.

The NRMSE does not have a standard form (the method of normalisation varies, e.g. by the mean value or by the total range), and it is less well defined for our particular case (where the mean is meaningless for an wave oscillating about zero, and the total range has no direct counterpart for complex values). We choose

to define $\chi$ as follows:

$$\chi = \frac{\sqrt{\frac{1}{C_N}\sum_{i=0}^{C_N}(\tilde{p}^i - \tilde{p}^i_{\mathrm{u}})\overline{(\tilde{p}^i - \tilde{p}^i_{\mathrm{u}})}}}{\mathrm{MaxDist}(\tilde{p})}, \tag{4.1}$$

where $\overline{(\tilde{p}^i - \tilde{p}^i_{\mathrm{u}})}$ is the complex conjugate of $(\tilde{p}^i - \tilde{p}^i_{\mathrm{u}})$, $C_N$ is the number of grid points outside the boundary layer, and $\tilde{p}^i$ is the value of the pressure at the $i$th grid point. The function MaxDist is a generalisation of the total range of a real-valued function, $\max(\cdot) - \min(\cdot)$. It is the maximum absolute distance between two coordinate pairs $\big(\mathrm{Re}\{\tilde{p}^i\}, \mathrm{Im}\{\tilde{p}^i\}\big)$, $\big(\mathrm{Re}\{\tilde{p}^j\}, \mathrm{Im}\{\tilde{p}^j\}\big)$; effectively the diameter of the smallest circle in the complex plane that contains all values of $\tilde{p}$.

For the 972 parameter sets tested inside the boundary layer (detailed in the caption of Table 1), the matching procedure described above was performed and the minimum matching $\chi$ calculated (i.e. the best-matched solution was found). The average $\chi$ of the best-matched uniform acoustics outside the boundary layer was found to be 0.0062% for $\tilde{p}$ and 0.14% for $\tilde{v}$. The matching of a viscous boundary layer to a inviscid uniform core flow is justified, in most cases, by these small errors.

## 5. Comparison of existing impedance boundary conditions

In the previous section it was shown that at the high Reynolds numbers we are considering, viscous effects on the acoustics are in general localised near the boundary. The acoustic pressure and velocity deviate from their inviscid counterparts either in the small acoustic boundary layer or over the base flow shear layer. Outside the base flow boundary layer, the acoustics are very well approximated by the correctly normalised uniform, inviscid solutions (which in cylindrical geometry are expressible in terms of Bessel functions, Eqs. (3.7), (3.8)). It was also evident that for certain sets of parameters, viscosity did not alter the acoustics even *inside* the boundary layer by much. So, models that collapse a sheared boundary layer into a boundary condition applicable to a uniform flow have merit. Here we compare three such boundary conditions to see when they should and should not be used.

Two inviscid conditions are tested: the Myers (or Ingard-Myers) condition [19,20], and the Modified Myers condition [6,7]. The Myers condition treats any base flow shear as a vortex sheet very close to the wall, and asserts zero flow on the wall side and uniform flow on the other. Continuity of acoustic pressure and displacement are assumed across the sheet. The Modified Myers condition models the bulk effects of the base flow shear layer by expanding in terms of a finite thickness boundary layer, capturing more of the physics of the problem. One viscous boundary condition is tested: that of Brambley [17], which is effectively the viscous Myers condition, and which must be calculated numerically. Not considered here are two other notable studies that suggest a viscous impedance boundary condition: those of Aúregan et. al. [16] and Nayfeh [15]. In Ref. 16, the velocity and temperature were restricted to having small variations across the boundary layer; in Ref. 15 only the acoustic boundary layer is considered rather than the base flow boundary layer. We thus only test Brambley's viscous condition, which does not have these restrictions (though, as will be shown, suffers from the same ill-posedness as does the Myers condition).

In order to compare the three conditions fairly, a tanh velocity profile is chosen,

$$U(r) = M\tanh\left(\frac{1-r}{\delta}\right) + M(1-\tanh(1/\delta))\left(\frac{1+\tanh(1/\delta)}{\delta}r + (1+r)\right)(1-r), \tag{5.1}$$

which can be exactly transformed to the boundary layer variable to calculate the viscous boundary condition [17]. For simplicity a constant density $\rho(r) \equiv 1$ is used.

First we look at the accuracy of $Z_{\mathrm{eff}}$ predictions. As shown in (3.9), we can calculate $Z_{\mathrm{eff}}$ analytically given the boundary impedance $Z$. To get $Z$ we solve the LNS for a given parameter set and then take $\tilde{p}(1)/\tilde{v}(1)$. This is the impedance that we pass to the three boundary conditions described above. They each output an effective impedance which we compare with the solution from (3.9). In Figure 7 the merit of both the first order inviscid, (b), and leading order viscous, (c), conditions can be seen, as both are improvements over the Myers condition, (a). The regions where the Myers condition is usefully accurate (warmer colours) are localised close to the origin. Accuracy is lost well within the plotted domain. The Modified Myers condition extends the region of accuracy down, and just off, the negative real line, but does not improve upon the Myers condition much in the right half plane. The leading order viscous condition

improves the accuracy more uniformly around the origin, but does not reach the high accuracies attained by the Modified Myers condition in most of the left half plane. This suggests that there are regions of $k$-space where viscosity is important, and regions where the inclusion of a finite thickness shear layer is important. At the higher Reynolds number ($5 \times 10^6$) and higher frequency ($\omega = 31$) shown in Figure 8, the effect of including viscosity is diminished – compare (a) and (c) – while the inclusion of a finite thickness shear layer still has an appreciable effect – compare (a) and (b).

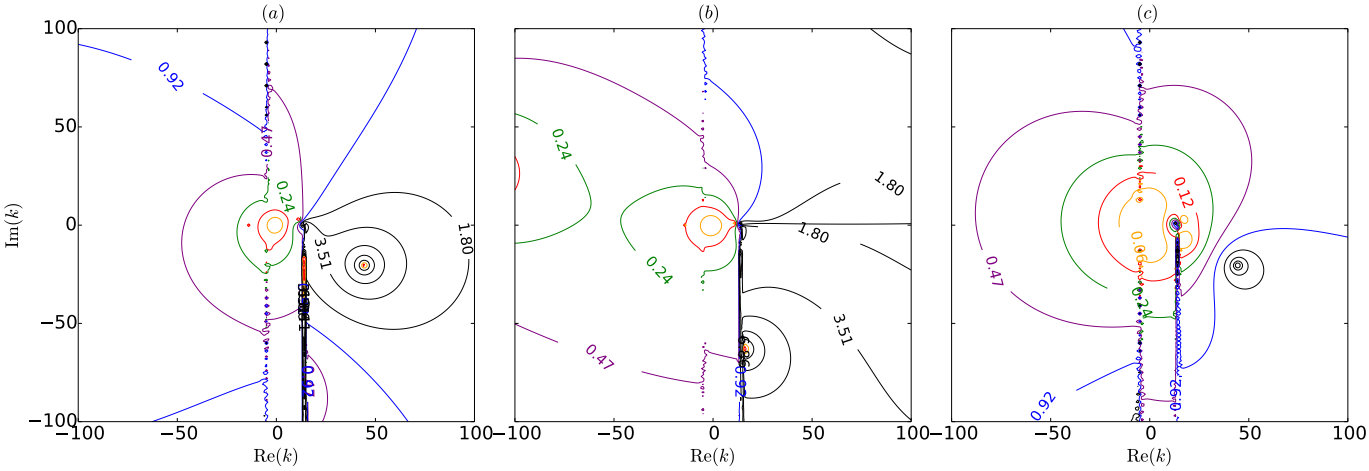


Figure 7. Contour plots in the complex $k$ plane showing the relative error of $Z_{\text{eff}}$ as predicted by the three impedance boundary condition models described in the main text. (a) is the Myers condition (leading order inviscid), (b) is the Modified Myers condition (first order inviscid), (c) is the leading order viscous Myers condition. The impedance at each point is taken from the LNS solution. $\omega = 7$, $M = 0.5$, $m = 12$, $\delta = 2 \times 10^{-3}$, $\text{Re} = 1 \times 10^6$. A tanh boundary layer profile is used, Eq. (5.1).

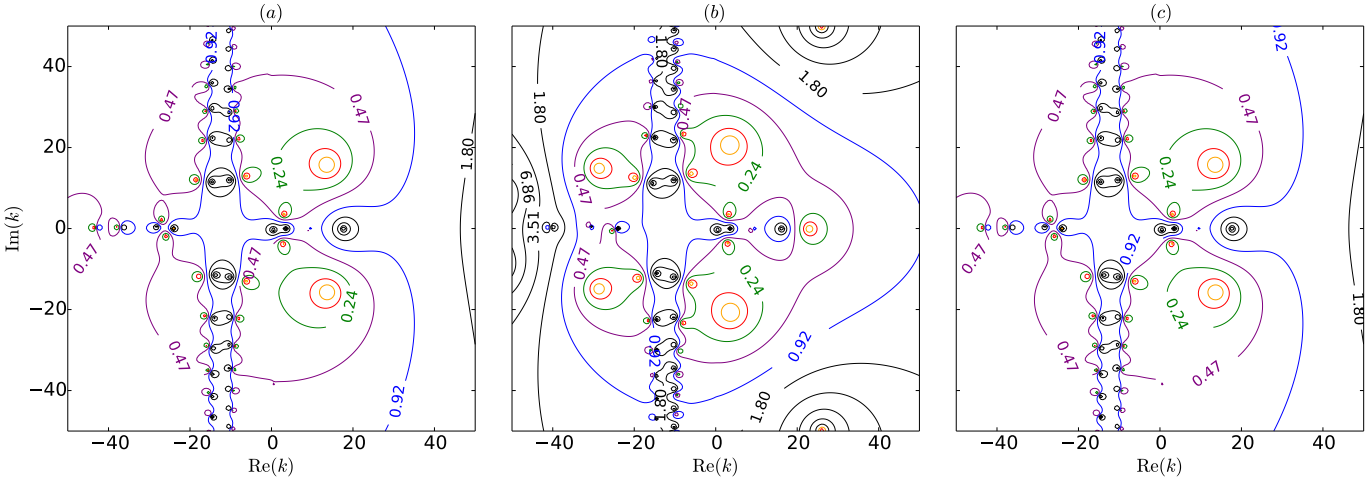


Figure 8. Contour plots in the complex $k$ plane showing the relative error of $Z_{\text{eff}}$ as predicted by the three impedance boundary condition models described in the main text. (a) is the Myers condition (leading order inviscid), (b) is the Modified Myers condition (first order inviscid), (c) is the leading order viscous Myers condition. The impedance at each point is taken from the LNS solution. $\omega = 31$, $M = 0.3$, $m = 24$, $\delta = 3 \times 10^{-2}$, $\text{Re} = 5 \times 10^6$. A tanh boundary layer profile is used, Eq. (5.1).

## A. Position of modes in the $k$-plane

Here we compare the three boundary conditions to the full LNS by looking at the position of modes in the complex $k$-plane. When a duct has a soft wall (a finite impedance) all modes have a non-zero imaginary part[22]. For stable modes, the sign of the imaginary part of the wavenumber tells us the direction of propagation of the decaying mode. A sheared boundary layer can support wave modes localised near the wall, known as surface modes[21]. These surface modes may become convectively unstable and grow in space[21–25].

In this case the imaginary part of the wavenumber tells us the growth rate of the unstable wave: a growing unstable wave propagating downstream has the same sign of $\mathrm{Im}(k)$ as a decaying wave propagating upstream when the frequency is purely real. Viscous and thermal dissipation are (usually) stabilising mechanisms, so the stability properties of surface modes for a fully viscous, sheared boundary layer can be expected to be different from those predicted by any existing effective impedance boundary conditions. Figure 9 shows the modes for $\omega = 5$, $m = 0$, and $\delta = 2 \times 10^{-3}$. The Reynolds number is chosen to satisfy the Blasius flat-plate scaling of $1/\delta^2$, such that $\mathrm{Re} = 2.5 \times 10^5$. Figure 9b shows the acoustic cutoff modes. There is an interesting contrast between upstream- and downstream-propagating modes: upstream-propagating modes ($\mathrm{Im}(k) > 0$) are more affected by viscosity (the leading order viscous modes are more accurate); while the downstream-propagating modes ($\mathrm{Im}(k) < 0$) are more affected by the finite-thickness shear layer (the Modified Myers modes are more accurate). Although the Myers condition seems to be performing comparatively well for the downstream-propagating modes, this does not hold for other parameter sets tested.

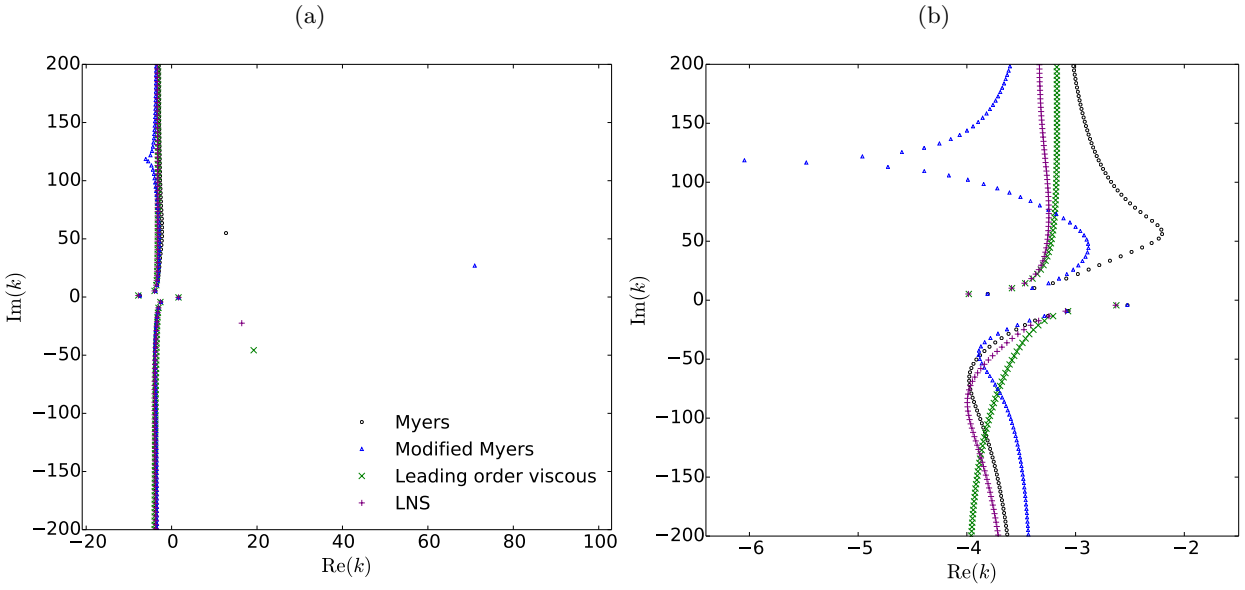


Figure 9. Modes in the $k$-plane for three effective impedance boundary conditions, and the LNS. $\omega = 5$, $m = 0$, $\delta = 2 \times 10^{-3}$, $\mathrm{Re} = 2.5 \times 10^5$ and $M = 0.5$. Impedance is modelled as a mass-spring-damper, $Z(\omega) = R + i\omega d - ib/\omega$, with parameters $R = 3$, $d = 0.15$, $b = 1.15$.

The right-most modes in Fig. 9a are surface modes. None of the existing boundary conditions accurately predict the LNS surface mode. Importantly, we see that the surface modes for the two viscous solutions (LNS and the leading order viscous boundary condition) have crossed the real $k$ axis. For the reasons mentioned above, this has ramifications for the stability of the mode. If the imaginary part of the frequency is reduced from zero to sufficiently negative, the movement of the mode in the $k$-plane should indicate whether it is stable or unstable (this is the Briggs-Bers stability criterion[37,38]). In Figure 10 the Modified Myers surface mode crosses the real axis, indicating that it is a downstream-propagating convective instability, as expected[7,8,21,25]. Also as expected, the Myers surface mode displays erroneous behaviour. The leading order viscous condition appears to qualitatively predict the behaviour of the LNS mode: The LNS surface mode does not cross the real axis, and hence remains stable. However, we need only plot the growth rate of the surface mode for the viscous boundary condition to see that it too predicts erroneous results. Figure 11 shows the growth rate of the unstable surface mode as it changes with real $k$. The modes for both the Myers and the leading order viscous conditions have unbounded growth rates. The Modified Myers condition regularises this problem and displays a bounded growth rate. The full behaviour of the LNS mode is not captured by any existing boundary condition, however. For small $k$ the LNS mode is stable; it destabilizes as $k$ is increased; for some finite $k$ the mode re-stabilizes.

It has been shown that the Myers condition is not sufficient in general for predicting acoustics in a viscous fluid. The two existing improvements on the Myers condition – the inclusion of a finite-thickness boundary layer, and the inclusion of viscothermal effects at leading order – both have merits, but neither capture the

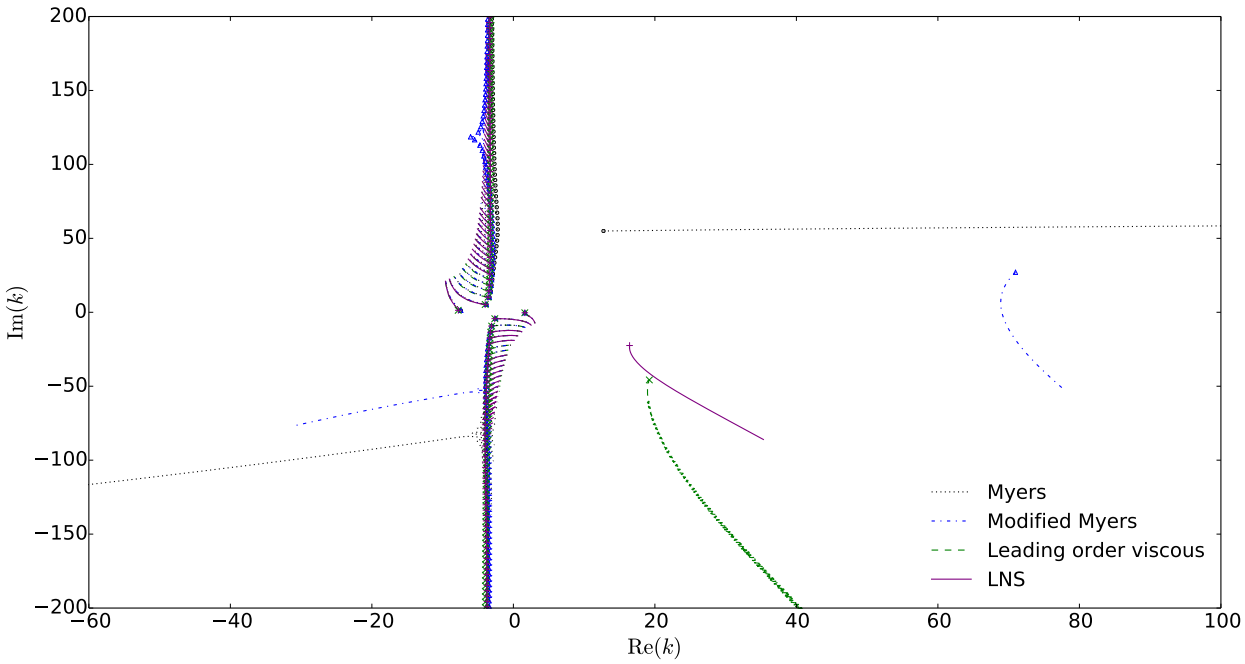


Figure 10. Modes in the $k$ plane as $\mathrm{Im}(\omega)$ is varied from 0 (points) to $-10$ with $\mathrm{Re}(\omega) = 5$ held fixed. Other parameters as in Figure 9.

full behaviour of the LNS.

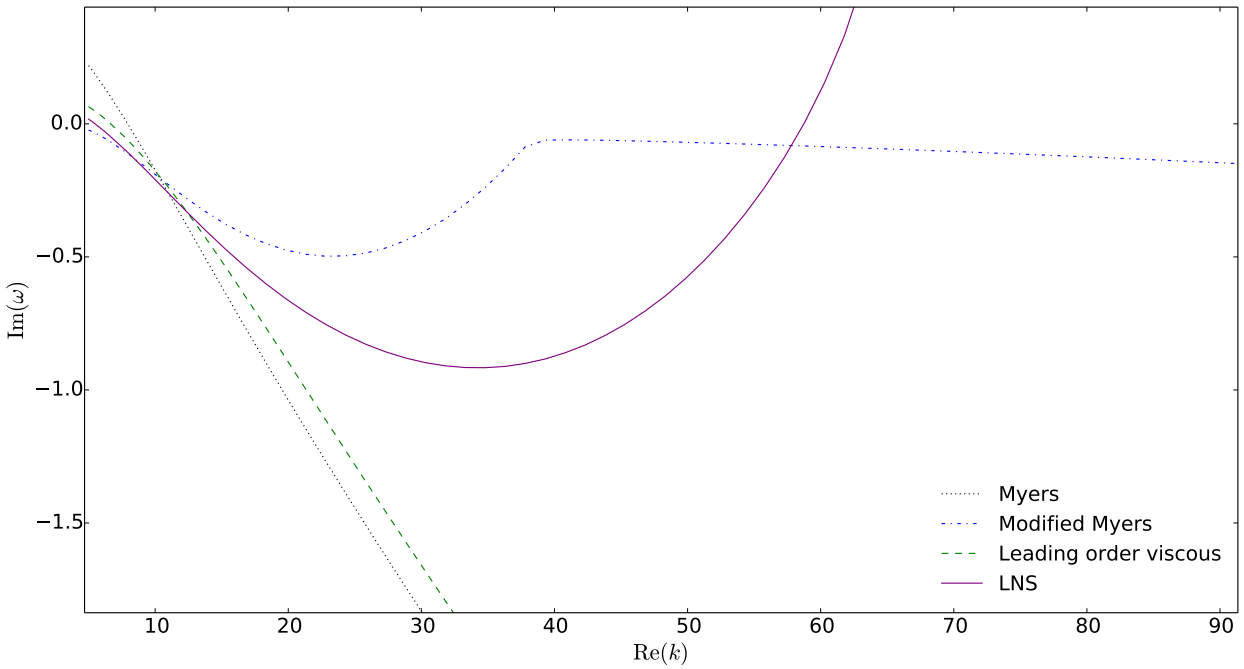


Figure 11. The evolution of the growth rate ($-\mathrm{Im}(\omega)$) of the unstable surface mode as $k$ (real) is increased. $m = 0$, $\delta = 7\times10^{-3}$, $\mathrm{Re} = 5 \times 10^6$ and $M = 0.5$. A tanh velocity profile is used (5.1). Liner impedance is modelled as a mass-spring-damper, $Z(\omega) = R + i\omega d - ib/\omega$, with parameters $R = 3$, $d = 0.15$, $b = 1.15$.

## 6. A new model for the effective impedance

In Section § 5 it was shown that none of the existing effective impedance boundary conditions capture fully the behaviour of a sheared, viscothermal boundary layer over an impedance lining. Here we address this issue by deriving a new boundary condition.

Consider a cylindrical duct with uniform, inviscid flow of Mach number $M$ in $0 \le r < 1-\delta$, and a sheared viscous boundary layer in $1 - \delta < r \le 1$. As in the LNS computations described above, in the boundary layer the base flow axial velocity, temperature and density follow some $r$-dependent profiles $U(r)$, $T(r)$ and $\rho(r)$, respectively. We use the Blasius flat-plate boundary layer scalings

$$r = 1 - \delta y, \qquad \xi \mathrm{Re} = 1/\delta^2, \qquad \delta\tilde{\tilde{v}} = \tilde{v}, \tag{6.1}$$

where $\xi$, nominally $\mathcal{O}(1)$, allows the decoupling of Re and $\delta$; and then make the helpful pre-emptive scalings

$$\hat{u} = \delta\tilde{u}, \qquad \hat{T} = \delta\tilde{T}, \qquad \hat{v} = \delta\tilde{\tilde{v}}. \tag{6.2}$$

These scalings allow the mass, momentum and energy equations to balance when expanded in terms of the boundary layer variable $y$. The pressure and azimuthal velocity remain $\mathcal{O}(1)$. Expanding Eqs. (2.3) and

retaining all terms up to $\mathcal{O}(\delta)$, the boundary layer perturbation equations become

$$i(\omega - Uk)\hat{T} + ikT\hat{u} - T^2\left(\frac{\hat{v}}{T}\right)_y = \delta\left[\gamma i(\omega - Uk)T\tilde{p} - T\hat{v} - imT\tilde{w}\right], \tag{6.3a}$$

$$i(\omega - Uk)\hat{u} + U_y\hat{v} - \xi(\gamma-1)^2T(T\hat{u}_y + U_y\hat{T})_y = \delta\left[i(\gamma-1)kT\tilde{p} - \xi(\gamma-1)^2T(T\hat{u}_y + U_y\hat{T})\right], \tag{6.3b}$$

$$\tilde{p}_y = \delta\left[2\xi(\gamma-1)(T\hat{v}_y)_y + \xi(\gamma-1)\left(\frac{\mu_B^*}{\mu^*} - \frac{2}{3}\right)(T\hat{v}_y - ikT\hat{u})_y - \frac{i(\omega-Uk)}{(\gamma-1)T}\hat{v} - i\xi(\gamma-1)k(T\hat{u}_y + U_y\hat{T})\right], \tag{6.3c}$$

$$\xi(T\tilde{w}_y)_y - \frac{i(\omega-Uk)}{(\gamma-1)^2T}\tilde{w} = -\frac{im}{\gamma-1}\tilde{p} + \mathcal{O}(\delta), \tag{6.3d}$$

$$i(\omega-Uk)\hat{T} + T_y\hat{v} - \frac{1}{\mathrm{Pr}}\xi(\gamma-1)^2T(T\hat{T})_{yy} - \xi(\gamma-1)^2T(U_y^2\hat{T} + 2TU_y\hat{u}_y) = \delta\left[(\gamma-1)i(\omega-Uk)T\tilde{p} - \frac{1}{\mathrm{Pr}}\xi(\gamma-1)^2T(T\hat{T})_y\right]. \tag{6.3e}$$

The viscothermal parameter $\xi$ takes the value $1/(\mathrm{Re}\delta^2)$, and tends to zero for inviscid flows. Equations (6.3) must be solved inside the boundary layer by assuming an expansion of the form $q = q^{(0)} + \delta q^{(1)} + \mathcal{O}(\delta^2)$ for the acoustic quantities. The solutions may then be matched to the inviscid acoustics (i.e. (3.7) and (3.8)) above in the limit $y \to \infty$.

### A. Boundary conditions

To write fully the boundary conditions that equations (6.3) satisfy we first need to understand what is happening at the transition between the viscous and inviscid regimes. Consider two cylindrical ducts, $A$ and $B$. Duct $A$ has uniform inviscid flow throughout, and $B$ has the flow regime we study here. Both $A$ and $B$ have the same core flow mach number, $M$. From the centreline of the ducts out to a radius of $r = 1 - \delta$ the acoustics in each duct are assumed to be identical (as justified in § B). The acoustic pressure and radial velocity in $A$, $p_u$ and $v_u$ respectively, may be expanded about the boundary:

$$p_u = p_\infty - \delta y p'_\infty + \mathcal{O}(\delta^2), \quad v_u = v_\infty - \delta y v'_\infty + \mathcal{O}(\delta^2), \tag{6.4}$$

where $p_\infty$ and $v_\infty$ are the values at the wall. The derivatives, derived from the Euler equations, are

$$p'_\infty = -i(\omega - Mk)v_\infty, \quad v'_\infty = \frac{(\omega-Mk)^2 - k^2 - m^2}{i(\omega-Mk)}p_\infty - v_\infty. \tag{6.5}$$

Now, if we choose a normalisation for $B$, our viscous system, by setting $\tilde{p}^{(0)} = 1$, and assert that the impedance boundary condition is satisfied exactly at leading order (that is, $\hat{v}^{(0)}(0) = -1/Z$) we cannot know anything about the normalisation of the inviscid system we are matching to (this would over-prescribe the system). In other words, the values $p_\infty$ and $v_\infty$ must have expansions in orders of $\delta$: $p_\infty = p_\infty^{(0)} + \delta p_\infty^{(1)}$ and $v_\infty = v_\infty^{(0)} + \delta v_\infty^{(1)}$. (In this way we ensure that $Z_{\mathrm{eff}} = p_\infty/v_\infty$ is calculated to first order.) Then, we match our solutions in $B$ to the uniform solutions in $A$ at infinity,

$$\begin{aligned}\tilde{p}(y) &= p_\infty - \delta y p'_\infty \\ &= p_\infty^{(0)} + \delta p_\infty^{(1)} + \delta y i(\omega + Mk)v_\infty^{(0)}, \qquad y \to \infty,\end{aligned} \tag{6.6a}$$

$$\begin{aligned}-\hat{v}(y) &= v_\infty - \delta y v'_\infty \\ &= v_\infty^{(0)} + \delta v_\infty^{(1)} + \delta y\left(v_\infty^{(0)} - \frac{(\omega-Mk)^2 - k^2 - m^2}{i(\omega-Mk)}p_\infty^{(0)}\right), \qquad y \to \infty.\end{aligned} \tag{6.6b}$$

The boundary conditions that correctly close the system, then, are

$$\begin{aligned}&\hat{u}^{(0)}(0) = 0, \quad \hat{T}^{(0)}(0) = 0, \quad -\hat{v}^{(0)}(0)Z = \tilde{p}^{(0)}, \quad \tilde{w}^{(0)}(0) = 0, \\ &\hat{u}^{(0)}(y) \to 0, \quad \hat{T}^{(0)}(y) \to 0, \quad \tilde{w}^{(0)} \to w_{\mathrm{u}} \quad \text{as} \quad y \to \infty,\end{aligned} \tag{6.7}$$

at $\mathcal{O}(1)$, and

$$\begin{aligned} \hat{u}^{(1)}(0) = 0, \quad \hat{T}^{(1)}(0) = 0, \quad \hat{v}^{(1)}(0) = 0, \\ \hat{u}^{(1)}(y) \to u_\mathrm{u}, \quad \hat{T}^{(1)}(y) \to T_\mathrm{u}, \quad \text{as} \quad y \to \infty, \end{aligned} \tag{6.8}$$

at $\mathcal{O}(\delta)$, along with the matching conditions described in (6.6).

### B. Numerical method

We solve the system (6.3), (6.7), and (6.8) in four parts. First, we choose the base flow (either the Blasius, § B, or tanh, (5.1), profiles from above). The leading order system for $\hat{u}^{(0)}$, $\hat{v}^{(0)}$ and $\hat{T}^{(0)}$ is discretized on the $y$ domain described in § B, with derivatives approximated using a fourth-order symmetric finite difference scheme. The linear system $A\mathbf{x} = \mathbf{b}$ is formed, where $A$ is a sparse banded $3N \times 3N$ matrix, and solved by a direct sparse solver to find the solution vector $\mathbf{x}$. We ensure that $A$ is not singular through the application of the inhomogeneous boundary condition $\hat{v}^{(0)}(0) = -\tilde{p}^{(0)}/Z$. The boundary conditions for $\hat{u}^{(0)}$ and $\hat{T}^{(0)}$ at infinity are applied at $y = Y$ by considering the solutions to the governing equations *outside* the boundary layer, for $y > Y$, where the equations decouple. Following Ref. 17, we find $\hat{u}^{(0)} \propto \exp\{-\eta y\}$, $\hat{T}^{(0)} \propto \exp\{-h\eta y\}$, where $h^2 = \mathrm{Pr}$ and $\eta^2 = i(\omega - Mk)$. The branch cut for $\eta$ must be chosen such that it is not real and negative. This ensures our solutions decay as $y \to \infty$. Thus, the boundary conditions that force decay at infinity are

$$\hat{u}^{(0)}_y + \eta \hat{u}^{(0)} = 0, \qquad \hat{T}^{(0)}_y + h\eta \hat{T}^{(0)} = 0.$$

After the solution has been found, the decoupled continuity equation for $y > Y$,

$$\hat{v}^{(0)}_y = i(\omega - Mk)(\gamma - 1)\hat{T}^{(0)} + ik\hat{u}^{(0)},$$

is used to extrapolate the value of $\hat{v}^{(0)}$ at $y = Y$ to $y = \infty$ (though the change is exponentially small, and usually outside the realms of the accuracy of the numerics).

Second, the first order correction to $\tilde{p}$ is calculated using solution to the leading order problem. From (6.3c) we find

$$\tilde{p}^{(1)} = 2(\gamma-1)T\hat{v}^{(0)}_y + (\gamma-1)\left(\frac{\mu^*_B}{\mu^*} - \frac{2}{3}\right)(T\hat{v}^{(0)}_y - ikT\hat{u}^{(0)}) - \int_0^y \frac{i(\omega - Uk)}{(\gamma-1)T}\hat{v}^{(0)} + i(\gamma-1)k(T\hat{u}_{0z} + U_z\hat{T})\mathrm{d}z, \tag{6.9}$$

where the integral may be performed numerically. From (6.9) we can see that only the second group of terms is affected by the value of the ratio $\mu^*_B/\mu^*$. We employ the continuity equation (6.3a) to rewrite these terms as

$$T(\hat{v}^{(0)}_y - ik\hat{u}^{(0)}) = i(\omega - Uk)\hat{T}^{(0)} + T_y\hat{v}^{(0)} + \mathcal{O}(\delta). \tag{6.10}$$

Now, at $y=0$, our boundary conditions (6.7) tell us $\hat{T}^{(0)}(0)=0$, while our assumption of thermal equilibrium between the wall and fluid forces $T_y(0)=0$. Hence the right hand side of (6.10) is always zero at the wall. As $y \to \infty$, we again have the boundary condition $\hat{T}^{(0)} \to 0$. Also, in this limit the base temperature is assumed to reach its constant core value, so $T_y=0$. So the right hand side of (6.10) is always zero at the edge of the boundary layer. The value of the $\mathcal{O}(\delta)$ correction to the pressure perturbation is thus only affected by the bulk viscosity in the interior of the boundary layer. Since the calculations of the effective impedance $Z_\mathrm{eff}$ only use the values of $\hat{v}$ and $\tilde{p}$ at the boundaries of the domain, it follows that the value of $Z_\mathrm{eff}$ will never be affected by a change in the bulk viscosity in this model. The mode shape of $\tilde{p}^{(1)}$ is changed, however, so one must be careful in using said shape in any analysis.

At this stage, the inhomogeneous $\tilde{w}$ equation, (6.3d), may be solved as a stand-alone problem for $\tilde{w}^{(0)}$, meaning the matrix $A$, above, may be reused at first order, with only the boundary condition rows having to be altered. Third, the leading order results are used as forcing on the right hand side of the first order problem. The boundary conditions at infinity are again applied at $y = Y$ by matching to solutions of the governing equations outside the boundary layer, in the uniform base flow region. This amounts to matching to the uniform flow values (those with the subscript 'u' in (6.7) and (6.8)) and making an exponentially

small adjustment. For completeness, at $y = Y$,

$$\tilde{w}_y^{(0)} + \eta\tilde{w}^{(0)} = \eta w_\mathrm{u}, \tag{6.11a}$$

$$\hat{u}^{(1)}(Y) = u_\mathrm{u} + \frac{1}{2}Y\hat{u}^{(0)}(Y) + a\mathrm{e}^{-\eta Y}, \tag{6.11b}$$

$$\hat{T}^{(1)}(Y) = T_\mathrm{u} + \frac{1}{2}Y\hat{T}^{(0)}(Y) + b\mathrm{e}^{-\eta h Y}, \tag{6.11c}$$

where $u_\mathrm{u} = k\tilde{p}^{(0)}/(\omega - Mk)$, $w_\mathrm{u} = m\tilde{p}^{(0)}/(\omega - Mk)$ and $T_\mathrm{u} = \tilde{p}^{(0)}$. The middle terms on the right hand sides of (6.11b) and (6.11c) are indeed exponentially small due to the boundary conditions at leading order.

Fourth, and finally, we use the matching principle described in (6.6) to find $p_\infty$ and $v_\infty$, the values of the acoustic pressure and radial velocity at the impedance wall of the associated inviscid, uniform base flow system. In this way we arrive at the effective impedance, $Z_\mathrm{eff} = p_\infty/v_\infty$, to first order in the boundary layer thickness, that, when applied at the wall of a duct with uniform inviscid flow, emulates the effects on the duct acoustics of a viscothermal boundary layer. The effective impedance may be applied using the Myers boundary condition[20], with the new $Z_\mathrm{eff}$ replacing the classical $Z_\mathrm{myers} = Z/(1 - Mk/\omega)$.

## C. Results

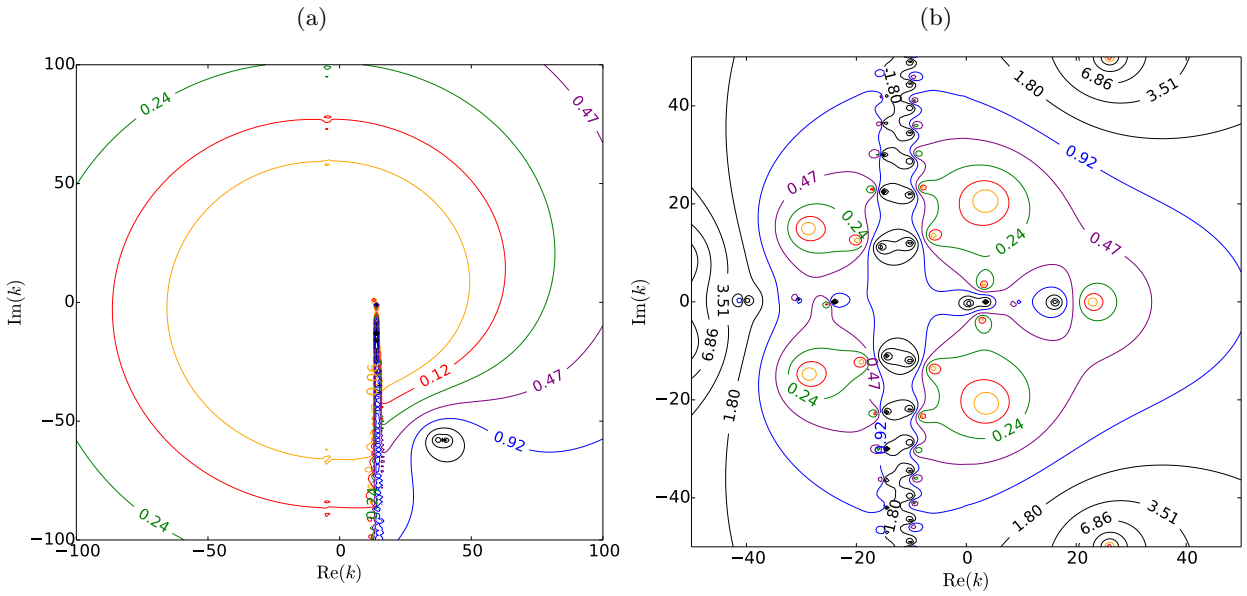


Figure 12. Contour plots in the complex $k$ plane showing the relative error of $Z_\mathrm{eff}$ as predicted by the new first order viscous impedance boundary condition. (a) $\omega = 7$, $M = 0.5$, $m = 12$, $\delta = 2 \times 10^{-3}$, $\mathrm{Re} = 1 \times 10^6$. (b) $\omega = 31$, $M = 0.3$, $m = 24$, $\delta = 3 \times 10^{-2}$, $\mathrm{Re} = 5 \times 10^6$. A tanh boundary layer profile is used in both plots, Eq. (5.1), and the impedance at each point is taken from the LNS solution.

The tests of the existing boundary conditions in § 5 are repeated here for the new boundary condition. First, the errors in $Z_\mathrm{eff}$ are plotted in Figure 12 for the parameter sets shown in Figures 7 and 8. At low frequency, the new condition performs brilliantly throughout the domain (Fig. 12a), allowing for the loss of accuracy in the anomalous region past the branch cut in the lower right quadrant. The improvement over the existing models is less pronounced at high frequency (Fig. 12b), but it is clear that the new model retains all of the positive parts of the Modified Myers and leading order viscous conditions. (Note: the poor performance in Fig. 12b is expected, as the derivation of the new condition assumes, like the existing models, that $k, \omega \ll 1/\delta$. For this plot, this means $k, \omega \ll 33$ for the model to be asymptotically valid. Hence, at the high frequency of $\omega = 31$, and near the edges of the $k$ domain, errors are expected.)

Second, the $k$-plane modes are plotted in Fig. 13. The new first order viscous model predicts the position of the surface mode exceptionally well (right-most modes, Fig. 13a), and both the upstream and downstream

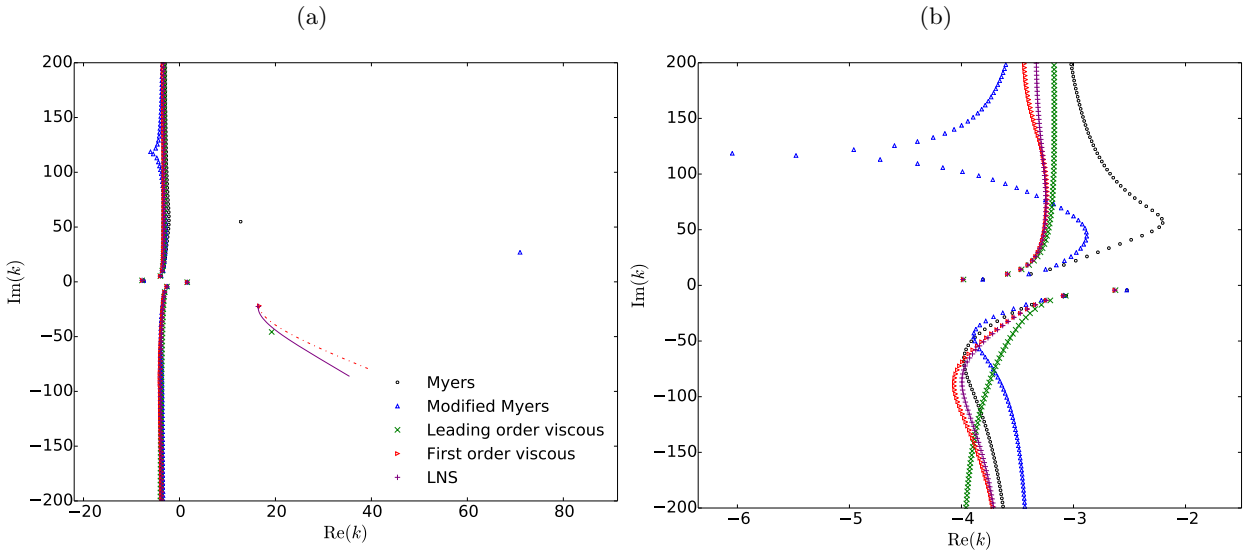


Figure 13. Modes in the $k$-plane for the new first order viscous condition, the three existing boundary conditions, and the LNS. $\omega = 5$, $m = 0$, $\delta = 2 \times 10^{-3}$, Re $= 2.5 \times 10^5$ and $M = 0.5$. Impedance is modelled as a mass-spring-damper, $Z(\omega) = R + i\omega d - ib/\omega$, with parameters $R = 3$, $d = 0.15$, $b = 1.15$. (a) shows two mode-tracks for the surface mode, as Im($\omega$) is reduced from zero to $-10$ with Re($\omega$) $= 5$ held fixed.

cutoff modes are more accurately reproduced (Fig. 13b). The surface mode of the new condition is traced in Fig. 13a as Im($\omega$) varies, and shows a much better agreement with the LNS mode than the existing conditions (c.f. Figure 10). Importantly, this suggests the new condition is capable of correctly modelling the stability of the surface waves supported by acoustic linings.

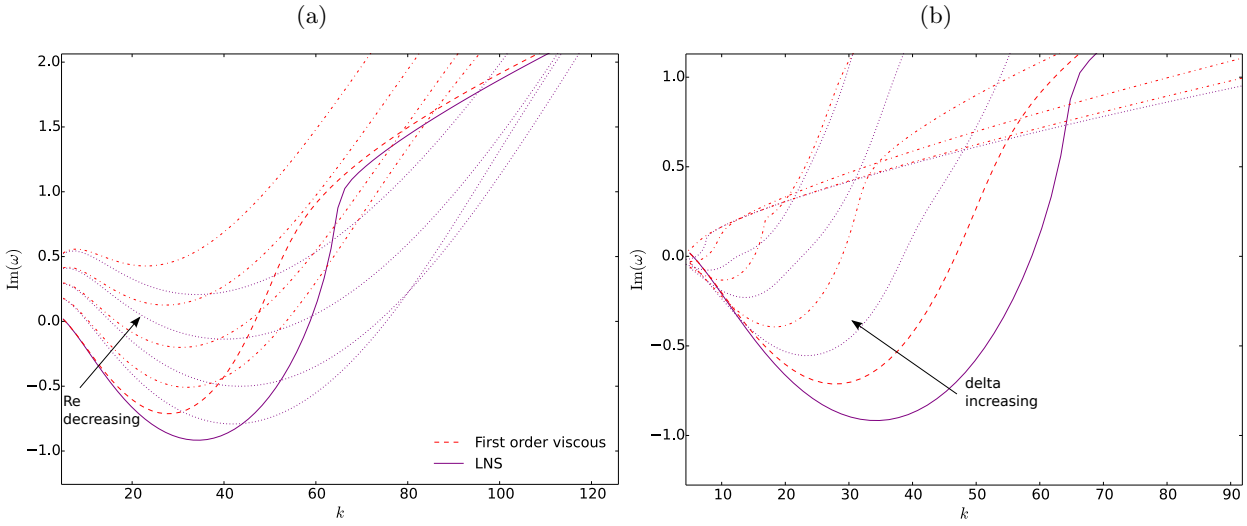


Figure 14. The growth rate of the unstable surface mode as $k$ (real) is increased, for the new first order viscous model (red, dashed then dash-dot) and the LNS (purple, solid then dotted). (a) Reynolds number is decreased from Re $= 5 \times 10^6$ through $1 \times 10^6$, $5 \times 10^5$, $3 \times 10^5$, $2 \times 10^5$ to $1 \times 10^5$ with $\delta = 7 \times 10^{-3}$ held fixed. (b) Boundary layer thickness is increased from $\delta = 7 \times 10^{-3}$ through $1 \times 10^{-2}$, $1.5 \times 10^{-2}$, $2 \times 10^{-2}$ to $2.5 \times 10^{-2}$ with Re $= 5 \times 10^6$ held fixed. In both cases, $m = 12$ and $M = 0.5$. Impedance is modelled as a mass-spring-damper, $Z(\omega) = R + i\omega d - ib/\omega$, with parameters $R = 3$, $d = 0.15$, $b = 1.15$.

Third, to explicitly investigate the stability, the behaviour of the possible instability mode is plotted in Figure 14 as Re and $\delta$ vary. We conjecture that the new condition may be used as a useful tool to investigate

the stability of the LNS near a lining: the qualitative behaviour of the mode is predicted correctly (the loss of accuracy as $k$ increases is expected, as described above). The agreement is not perfect, though, as shown by the second-to-last (as Re is decreased) mode in Fig. 14a which is unstable for the LNS for stable for the new model. This does not diminish the great improvement of the new model over the existing ones, however.

Figure 14 hints at an interesting relationship between Re and $\delta$ as parameters which govern the linear stability of a mode. In inviscid studies this is wholly lost, and the unstable mode remains theoretically unstable. Here, however, the separation of the two parameters allows their effect to be viewed independently.

## 7. Concluding remarks

This paper has tackled four questions: whether viscosity is important for calculating the acoustics in a sheared boundary layer at a lined wall; whether near-wall effects really are localised to the wall, such that a boundary condition on a uniform flow can be applied; whether existing effective impedance boundary conditions capture the true behaviour of viscous, sheared acoustics; and whether a new boundary condition can be derived which does just that.

By comparing solutions of the Linearised Navier–Stokes (LNS) and Pridmore-Brown equations inside the base flow boundary layer, it was found that the errors associated with using inviscid equations is appreciably large, and that viscothermal effects can sometimes be as important as shear. For the 972 parameter sets tested, the Normalised Root Mean Square Error (NRMSE) of the inviscid acoustics compared with the viscous acoustics over the boundary layer averaged 6.8% for the radial velocity and 1.6% for the pressure (with the proviso that the acoustic pressure satisfied the same boundary condition for the viscous and inviscid computations, so the error was suppressed). Often the NRMSE rose above 10% (in 143 of the 972 test cases). One result of this bulk testing was the discovery of a trend linking increased Mach number to increased inviscid error. Another trend was that lower frequency acoustics were more effected by viscosity. These two trends were suggested in the experimental study Ref. 39, and support the results of Ref. 16, in which it was found that the inviscid Myers condition was recovered from an asymptotic viscous boundary condition only at high frequency. Note that a Helmholtz number of $\omega = 5$ is small in this case.

Outside the boundary layer, where the shear is small or zero, the mode shapes of the viscous acoustics were matched to the analytic expressions for the uniform inviscid acoustics. For the same 972 parameter sets, the average NRMSE of the uniform invsicid acoustics outside the boundary layer was found to be 0.0062% for the pressure and 0.14% for the radial velocity. These low errors suggest that applying a boundary condition to a uniform slipping flow instead of modelling the sheared, viscous boundary layer is warranted. The near-wall effects of shear and viscosity do not penetrate far into the duct, with only 26 of the 972 test cases having an average error of more than 1% throughout the duct.

Three existing effective impedance boundary conditions were tested against LNS computations. The Myers condition [19,20], known to be illposed [18] and fallible when compared with experiments [12–14], was shown to be inadequate in its effective impedance predictions except in small, isolated regions of wavenumber space, usually near the origin. It is unsuitable for predicting the stability of surface modes, but for its simplicity it approximates acoustic cutoff modes fairly well. The Modified Myers condition [6,7] is an inviscid condition that takes into account the finite thickness of the base flow boundary layer. It is well-posed, and as such can be used to predict the stability of surface modes. However, it was shown that viscous dissipation plays an important role in determining the stability of surface modes, hence the inviscid Modified Myers condition does not capture the possibility of a mode restabilizing at high wavenumbers or low Reynolds numbers. The leading order viscous condition [17] was shown also to be illposed, and hence unsuitable for stability studies, despite its improvement over the inviscid models in predicting upstream-propagating cutoff modes. The result stemming from these comparisons is that neither viscosity nor a finite-thickness shear layer alone are enough to fully capture the behaviour of viscous sheared acoustics as calculated by the Linearised Navier–Stokes equations. Hence, no existing boundary condition is the complete package.

To rectify this problem, the paper culminated in its main result: a new boundary layer expansion of the Navier–Stokes equations in the small boundary layer thickness $\delta$, leading to a system of equations that may be solved numerically to calculate the effective impedance of a viscothermal boundary layer over an acoustic lining. The new condition was shown to agree extremely well with the full numerics in all tests. It is an improvement over the existing boundary conditions for predicting the position of cutoff and surface modes; for studying mode stability and approximating maximum instability growth rates; and for straightforward effective impedance calculations. Although no analytic form for the boundary condition is found, the derived

system of equations could be efficiently incorporated into a boundary solver without much computational cost. Work on finding approximate analytic forms of the new boundary condition, for different boundary layer scalings or parameter limits, is ongoing.

## References


[1] Brambley, E. J. and Peake, N., "Stability and acoustic scattering in a cylindrical thin shell containing compressible mean flow," *Journal of Fluid Mechanics*, Vol. 602, 2008, pp. 403–426.

[2] Mungur, P. and Gladwell, G. M. L., "Acoustic wave propagation in a sheared fluid contained in a duct," *Journal of Sound and Vibration*, Vol. 9, No. 1, 1969, pp. 28–48.

[3] Jones, D. S., "The Scattering of Sound by a Simple Shear Layer," *Phil. Trans. R. Soc.*, Vol. 284, 1977, pp. 287–328.

[4] Tester, B. J., "Some Aspects of "Sound" Attenuation in Lined Ducts containing Inviscid Mean Flows with Boundary Layers," *Journal of Sound and Vibration*, Vol. 28, 1973, pp. 217–245.

[5] Eversman, W. and Beckemeyer, R. J., "Transmission of Sound in Ducts with Thin Shear Layer – Convergence to the Uniform Flow Case," *Journal of the Acoustical Society of America*, Vol. 52, No. 1B, 1972, pp. 216–220.

[6] Myers, M. K. and Chuang, S. L., "Uniform Asymptotic Approximations for Duct Acoustic Modes in a Thin Boundary-Layer Flow," *AIAA Journal*, Vol. 22, No. 9, 1984, pp. 1234–1241.

[7] Brambley, E. J., "Well-Posed Boundary Condition for Acoustic Liners in Straight Ducts with Flow," *AIAA Journal*, Vol. 49, No. 6, 2011, pp. 1272–1282.

[8] Rienstra, S. W. and Darau, M., "Boundary-layer thickness effects of the hydrodynamic instability along an impedance wall," *Journal of Fluid Mechanics*, Vol. 671, 2011, pp. 559–573.

[9] Jones, M. G., Watson, W. R., and Parrott, T. L., "Benchmark Data for Evaluation of Aeroacoustic Propagation Codes with Grazing Flow," *11th AIAA/CEAS Aeroacoustics Conference*, American Institute of Aeronautics and Astronautics, May 2005.

[10] Burak, M., Billson, M., Eriksson, L.-E., and Baralon, S., "Validation of a Time & Frequency Domain Grazing Flow Acoustic Liner Model," *14th AIAA/CEAS Aeroacoustics Conference (29th AIAA Aeroacoustics Conference)*[40].

[11] Burak, M. O., Billson, M., Eriksson, L.-E., and Baralon, S., "Validation of a Time- and Frequency-Domain Grazing Flow Acoustic Liner Model," *AIAA Journal*, Vol. 47, No. 8, 2009, pp. 1841–1848.

[12] Aurégan, Y. and Leroux, M., "Experimental evidence of an instability over an impedance wall in a duct with flow," *Journal of Sound and Vibration*, Vol. 317, 2008, pp. 432–439.

[13] Marx, D., Aurégan, Y., Bailliet, H., and Valiére, J.-C., "PIV and LDV evidence of hydrodynamic instability over a liner in a duct with flow," *Journal of Sound and Vibration*, Vol. 329, 2010, pp. 3798–3812.

[14] Renou, Y. and Aurégan, Y., "Failure of the Ingard-Myers boundary condition for a lined duct: An experimental investigation," *Journal of the Acoustical Society of America*, Vol. 130, No. 1, 2011, pp. 52–60.

[15] Nayfeh, A. H., "Effect of the acoustic boundary layer on the wave propagation in ducts," *J. Acoust. Soc. Am.*, Vol. 54, 1973, pp. 1737–1742.

[16] Aurégan, Y., Starobinski, R., and Pagneux, V., "Influence of grazing flow and dissipation effects on the acoustic boundary conditions at a lined wall," *The Journal of the Acoustical Society of America*, Vol. 109, No. 1, 2001, pp. 59–64.

[17] Brambley, E. J., "Acoustic implications of a thin viscous boundary layer over a compliant surface or permeable liner," *Journal of Fluid Mechanics*, Vol. 678, 7 2011, pp. 348–378.

[18] Brambley, E. J., "Fundamental problems with the model of uniform flow over acoustic linings," *Journal of Sound and Vibration*, Vol. 322, 2009, pp. 1026–1037.

[19] Ingard, U., "Influence of fluid motion past a plane boundary on sound reflection, absorption, and transmission," *Journal of the Acoustical Society of America*, Vol. 31, 1959, pp. 1035–1036.

[20] Myers, M., "On the acoustic boundary condition in the presence of flow," *Journal of Sound and Vibration*, Vol. 71, No. 3, 1980, pp. 429–434.

[21] Rienstra, S. W., "A Classification of Duct Modes Based on Surface Waves," *Wave Motion*, Vol. 37, No. 2, 2003, pp. 119–135.

[22] Brambley, E. J. and Peake, N., "Classification of aeroacoustically relevant surface modes in cylindrical lined ducts," *Wave Motion*, Vol. 43, 2006, pp. 301–310.

[23] Vilenksi, G. G. and Rienstra, S., "On hydrodynamic and acoustic modes in a ducted shear flow with wall lining," *Journal of Fluid Mechanics*, Vol. 583, 2007, pp. 45–70.
[24] Vilenski, G. G. and Rienstra, S. W., "Numerical Study of Acoustic Modes in Ducted Shear Flow," *Journal of Sound and Vibration*, Vol. 307, No. 3–5, 2007, pp. 610–626.
[25] Brambley, E. J., "Surface modes in sheared boundary layers over impedance linings," *Journal of Sound and Vibration*, Vol. 332, 2013, pp. 3750–3767.
[26] Boyer, G., Piot, E., and Brazier, J.-P., "Theoretical investigation of hydrodynamic surface mode in a lined duct with sheared flow and comparison with experiment," *Journal of Sound and Vibration*, Vol. 330, 2011, pp. 1793–1809.
[27] Tritton, D., *Physical Fluid Dynamics*, Oxford Science Publications, Clarendon Press, 1988.
[28] Landau, L. and Lifshitz, E., *Fluid Mechanics*, Elsevier, New York, 2nd ed., 1987.
[29] Stewart, H. J., "The Energy Equation for a Viscous Compressible Fluid," *Proc Natl Acad Sci USA*, Vol. 28, No. 5, 1942, pp. 161–164.
[30] Brambley, E. J., "DRP schemes perform badly for decaying or growing oscillations," *21st AIAA/CEAS Aeroacoustics Conference and Exhibit*, American Institute of Aeronautics and Astronautics, June 2015.
[31] Nayfeh, A. H., Kaiser, J. E., and Shaker, B. S., "Effect of mean-velocity profile shapes on sound transmission through two-dimensional ducts," *Journal of Sound and Vibration*, Vol. 34, No. 3, 1974, pp. 413–423.
[32] Gabard, G., "A comparison of impedance boundary conditions for flow acoustics," *Journal of Sound and Vibration*, Vol. 332, No. 4, February 2013, pp. 714–724.
[33] Schlichting, H. and Gersten, K., *Boundary-Layer Theory*, Physic and astronomy, MacGraw-Hill, 2000.
[34] Brambley, E. J., "Viscous boundary layer effects on the Myers impedance boundary condition," *15th AIAA/CEAS Aeroacoustics Conference*, American Institute of Aeronautics and Astronautics, March 2009.
[35] Rienstra, S. W. and Vilenksi, G. G., "A Systematic Impedance Model for Non-Linear Helmholtz Resonator Liner," *14th AIAA/CEAS Aeroacoustics Conference (29th AIAA Aeroacoustics Conference)*[40].
[36] Pridmore-Brown, D., "Sound Propagation in a Fluid Flowing Through an Attenuating Duct," *Journal of Fluid Mechanics*, Vol. 4, No. 4, 1958, pp. 393–406.
[37] Briggs, R. J., *Electron-stream Interaction with Plasmas*, MIT, 1964.
[38] Bers, A., "Space-time evolution of plasma instabilitiesabsolute and convective," *Basic Plasma Physics, Handbook of Plasma Physics, Vol. 1*, edited by A. A. Galeev and R. N. Sudan, North-Holland, 1983, pp. 451–517.
[39] Watson, W. and Jones, M., "Evaluation of Wall Boundary Conditions for Impedance Eduction Using a Dual-Source Method," *14th AIAA/CEAS Aeroacoustics Conference (33rd AIAA Aeroacoustics Conference*, American Institute of Aeronautics and Astronautics, June 2012.
[40] *14th AIAA/CEAS Aeroacoustics Conference (29th AIAA Aeroacoustics Conference)*. American Institute of Aeronautics and Astronautics, May 2008.